Cellular/Molecular

# The NGF$^{R100W}$ Mutation Specifically Impairs Nociception without Affecting Cognitive Performance in a Mouse Model of Hereditary Sensory and Autonomic Neuropathy Type V

**Giovanna Testa,[1] Marco Mainardi,[1] Chiara Morelli,[2,3] Francesco Olimpico,[1] Laura Pancrazi,[1,4] Carla Petrella,[5] Cinzia Severini,[5] Rita Florio,[6] Francesca Malerba,[6] Antonia Stefanov,[4] Enrica Strettoi,[4] Rossella Brandi,[6] Ivan Arisi,[6] Paul Heppenstall,[2] Mario Costa,[4] Simona Capsoni,[1,7] and Antonino Cattaneo[1,6]**

[1]Bio@SNS, Scuola Normale Superiore, 56124 Pisa, Italy, [2]European Molecular Biology Laboratory (EMBL), 00015 Monterotondo (Rome), Italy, [3]EMBL International PhD Programme, Faculty of Biosciences, Heidelberg University, 69120 Heidelberg, Germany, [4]Institute of Neuroscience, National Research Council (CNR), 56124 Pisa, Italy, [5]Institute of Biochemistry and Cell Biology (IBBC), CNR, DOS Policlinico Umberto I, 00161 Rome, Italy, [6]Neurotrophins and Neurodegenerative Diseases Laboratory, Rita Levi-Montalcini European Brain Research Institute (EBRI), 00161 Rome, Italy, and [7]Institute of Physiology, Department of Biomedical and Specialty Surgical Sciences, University of Ferrara, 44121 Ferrara, Italy

Nerve growth factor (NGF) is a key mediator of nociception, acting during the development and differentiation of dorsal root ganglion (DRG) neurons, and on adult DRG neuron sensitization to painful stimuli. NGF also has central actions in the brain, where it regulates the phenotypic maintenance of cholinergic neurons. The physiological function of NGF as a pain mediator is altered in patients with Hereditary Sensory and Autonomic Neuropathy type V (HSAN V), caused by the 661C>T transition in the *Ngf* gene, resulting in the R100W missense mutation in mature NGF. Homozygous HSAN V patients present with congenital pain insensitivity, but are cognitively normal. This led us to hypothesize that the R100W mutation may differentially affect the central and peripheral actions of NGF. To test this hypothesis and provide a mechanistic basis to the HSAN V phenotype, we generated transgenic mice harboring the human 661C>T mutation in the *Ngf* gene and studied both males and females. We demonstrate that heterozygous NGF$^{R100W/wt}$ mice display impaired nociception. DRG neurons of NGF$^{R100W/wt}$ mice are morphologically normal, with no alteration in the different DRG subpopulations, whereas skin innervation is reduced. The NGF$^{R100W}$ protein has reduced capability to activate pain-specific signaling, paralleling its reduced ability to induce mechanical allodynia. Surprisingly, however, NGF$^{R100W/wt}$ mice, unlike heterozygous mNGF$^{+/-}$ mice, show no learning or memory deficits, despite a reduction in secretion and brain levels of NGF. The results exclude haploinsufficiency of NGF as a mechanistic cause for heterozygous HSAN V mice and demonstrate a specific effect of the R100W mutation on nociception.

*Key words:* allodynia; dorsal root ganglia; hereditary sensory and autonomic neuropathy type V; learning and memory; nerve growth factor; skin innervation

**Significance Statement**

The R100W mutation in nerve growth factor (NGF) causes Hereditary Sensory and Autonomic Neuropathy type V, a rare disease characterized by impaired nociception, even in apparently clinically silent heterozygotes. For the first time, we generated and characterized heterozygous knock-in mice carrying the human R100W-mutated allele (NGF$^{R100W/wt}$). Mutant mice have normal nociceptor populations, which, however, display decreased activation of pain transduction pathways. NGF$^{R100W}$ interferes with peripheral and central NGF bioavailability, but this does not impact on CNS function, as demonstrated by normal learning and memory, in contrast with heterozygous NGF knock-out mice. Thus, a point mutation allows neurotrophic and pronociceptive functions of NGF to be split, with interesting implications for the treatment of chronic pain.

## Introduction

Nerve growth factor (NGF; Levi-Montalcini, 1987), in addition to its classical neurotrophic actions, is an established mediator of pain pathophysiology. Indeed, NGF is a key molecule in the pain machinery, with powerful proinflammatory and sensitizing actions (Denk et al., 2017). NGF regulates pain perception in humans and pain-related behavioral responses in animals; injections of NGF in animals (Lewin et al., 1993) and humans (Svensson et al., 2003) elicit rapid and long-lasting hyperalgesia, while NGF-neutralizing molecules are effective analgesics in many models of persistent pain (McMahon et al., 1995; Ugolini et al., 2007). NGF is strategically positioned to regulate pain, acting on both nociceptors (Lewin et al., 2014) and attraction of immune cells at injury sites (Levi-Montalcini et al., 1996; Skaper, 2017). NGF levels increase in affected tissues in various experimental or pathological inflammatory conditions (Minnone et al., 2017). Based on this, anti-NGF antibodies are being clinically evaluated to alleviate chronic pain (e.g., due to osteoarthritis; Lane et al., 2010). On the other hand, its robust neurotrophic properties have led to testing NGF as a therapeutic candidate for different conditions including diabetic polyneuropathy (Apfel et al., 1994; Pittenger and Vinik, 2003) and neurodegenerative diseases (Mitra et al., 2019). However, these trials failed due to significant adverse effects, including NGF-induced pain (Apfel, 2002). Thus, elucidating NGF actions on pain transmission, also taking into account signaling through TrkA and p75$^{NTR}$, would be a step toward overcoming these limitations.

In this regard, Hereditary Sensory Autonomic Neuropathies (HSANs) are rare congenital pain insensitivity diseases that offer an opportunity to dissect NGF roles in pain. Indeed, several mutations leading to pain insensitivity have been described in the genes encoding NGF and TrkA (tropomyosin receptor kinase A; Indo, 2001; Capsoni, 2014; Nahorski et al., 2015). For example, recessive mutations in the TrkA gene cause HSAN IV, characterized by insensitivity to pain, autonomic defects, and mental retardation (Indo, 2001). A Swedish family suffering from severe loss of pain, leading to frequent bone fractures and Charcot joints, was discovered to carry, instead, the 661C>T transition in the *NGFb* gene, resulting in the R100W mutation in mature NGF. This "painlessness" disorder was called HSAN V (Einarsdottir et al., 2004). Compared with HSAN IV patients, homozygous HSAN V patients display a similar congenital indifference to noxious stimuli, but no cognitive deficits (Einarsdottir et al., 2004). In contrast, heterozygous carriers, despite reduced skin innervation and unmyelinated fiber number, along with altered thermoception, do not present with readily detectable clinical signs and have been identified only through pedigree and genetic screening (Axelsson et al., 2009; Minde et al., 2009; Perini et al., 2016).

We and others have shown that the NGF$^{R100W}$ protein displays reduced binding to, and signaling via, p75$^{NTR}$, whereas interaction with TrkA is unaffected (Covaceuszach et al., 2010; Capsoni et al., 2011; Sung et al., 2018). Thus, we proposed that NGF$^{R100W}$, with its biased TrkA agonist receptor profile (Covaceuszach et al., 2010; Capsoni et al., 2011), might help in dissecting trophic and nociceptive actions of NGF. To elucidate how these molecular features concur to determine the clinical HSAN V phenotype, we describe here the characterization of a mouse knock-in line harboring the NGF$^{R100W}$ mutation. We focused on heterozygous NGF$^{R100W/wt}$ mice, since homozygous NGF$^{R100W/R100W}$ mice die by the first month of life (Testa et al., 2019).

We demonstrate that heterozygous NGF$^{R100W/wt}$ mice display impaired nociception, despite having normal dorsal root ganglion (DRG) neurons. The NGF$^{R100W}$ protein has a reduced capability to activate pain-specific signaling, correlating with a reduced ability to induce mechanical allodynia. Surprisingly, however, NGF$^{R100W/wt}$ mice, unlike heterozygous mNGF$^{+/-}$ mice, show no learning or memory deficits, despite reduced NGF secretion. Together, our results provide significant insights into the molecular pathogenesis of the HSAN V phenotype and demonstrate a specific effect of NGF$^{R100W}$ on nociception, with no impact on cognitive performance. These features make NGF$^{R100W}$ an attractive tool to manipulate pain sensitivity and to exert neurotrophic actions in the absence of pain sensitization effects.

## Materials and Methods

*Ethics statement on mouse experiments.* All animal procedures were approved by the Italian Ministry of Health and were fully compliant with Italian (Ministry of Health guidelines, Legislative Decree n°26/2014) and European Union (Directive n°2010/63/UE) laws on animal research. The experiments were performed in strict accordance with the ARRIVE guidelines (Animal Research: Reporting in Vivo Experiments). In addition, the principles of the Basel Declaration, including the "3R" concept, have been considered throughout the whole project. Both male and female mice were used in this study.

*Generation of knock-in human NGF$^{R100W/wt}$ mice.* pCMV6-XL5-human NGF$^{wt}$ plasmid was obtained from OriGene (catalog #SC123827) and pCMV6-XL5-human NGF$^{R100W}$ was generated using site-specific mutagenesis PCR. The targeting constructs were generated using classical cloning technologies. Briefly, a BAC (bacterial artificial chromosome; clone RP24-160F12) containing the entire regions of interest flanking the NGF sequence, was used to generate intermediate plasmids by cloning in pBluescript SK(−) the 5′ homology arm (from 89489 to 94076, restriction site MfeI) and 3′ homology arm (from 94803 to 99710, restriction site HindIII). The human NGF$^{R100W}$ coding sequence was cloned in the pKO2.1 targeting vector carrying the DTA (diptheria toxin A) negative selection cassette (provided by Dr. L. Ronfani, San Raffaele Hospital, Milan, Italy). The targeting vector was transfected into R1p.15 cells (background SV129), and positive clones were selected using neomycin resistance.

*Southern blot analysis.* Genomic DNA was extracted by means of phenol:chloroform:isoamyl alcohol from ~350 cell clones electroporated with NGF$^{R100W}$ targeting vector. The purified DNA was first incubated with EcoRI (for 5′ screening), then positive clones were confirmed by XbaI digestion (for 3′ screening). Digestions were run in a 0.8% agarose gel overnight (O/N) at 50 V. After a mild depurination and denaturation, gels were blotted on nitrocellulose and filters were incubated with an external 5′ or 3′ probe. The 5′ probe labels a 10.7 kb EcoRI band in the wild-type (WT) allele and a 5.2 kb EcoRI band in recombinant allele (Fig. 1*A*). The 3′ probe labels an 8 kb XbaI band in the WT allele and a 12.7 kb XbaI band in the recombinant allele (Fig. 1*B*).

Received March 26, 2019; revised Oct. 1, 2019; accepted Oct. 27, 2019.

Author contributions: M.C., S.C., and A.C. designed research; G.T., M.M., C.M., F.O., L.P., C.P., C.S., A.S., E.S., R.B., P.H., and S.C. performed research; R.F. and F.M. contributed unpublished reagents/analytic tools; G.T., M.M., A.S., and I.A. analyzed data; G.T., M.M., S.C., and A.C. wrote the paper.

This work was supported by the EU FP7 PAINCAGE project (Grant 603191, to A.C.), by Fondazione Telethon (Grant GGP11179, to A.C.), by European Union's Horizon 2020 research funds under the Marie Skłodowska-Curie (Grant 674901, to A.S. and E.S.), and by MIUR_PRIN17 project (Grant 2017HPTFFC_001, to A.C.). We thank Lorenza Ronfani, Rosanna Rinaldi, and Ivana Benzoni (San Raffaele Hospital, Milan, Italy); Mara D'Onofrio (Rita Levi-Montalcini European Brain Research Institute); laboratory members Maria Antonietta Calvello, Vania Liverani, Nicola Maria Carucci, Francesco Gobbo, Caterina Rizzi, Alessandro Viegi, and Alexia Tiberi (BioSNS, Scuola Normale Superiore) for their help and support; Elena Novelli (Institute of Neuroscience, CNR) for valuable technical help; Nicola Origlia (Institute of Neuroscience, CNR) for support in electrophysiology experiments; Enrico Pracucci and Gian Michele Ratto [NEST (National Enterprise for nanoScience and nanoTechnology) Laboratory, Scuola Normale Superiore] for support in DRG sectioning; Irene Perini and India Morrison (Linköping University, Linköping, Sweden) or useful discussions; and Moses W. Chao (New York University, New York, NY) for useful discussion and critical reading of the manuscript.

The authors declare no competing financial interests.

Correspondence should be addressed to Antonino Cattaneo at antonino.cattaneo@sns.it or Simona Capsoni at simona.capsoni@sns.it.

https://doi.org/10.1523/JNEUROSCI.0688-19.2019

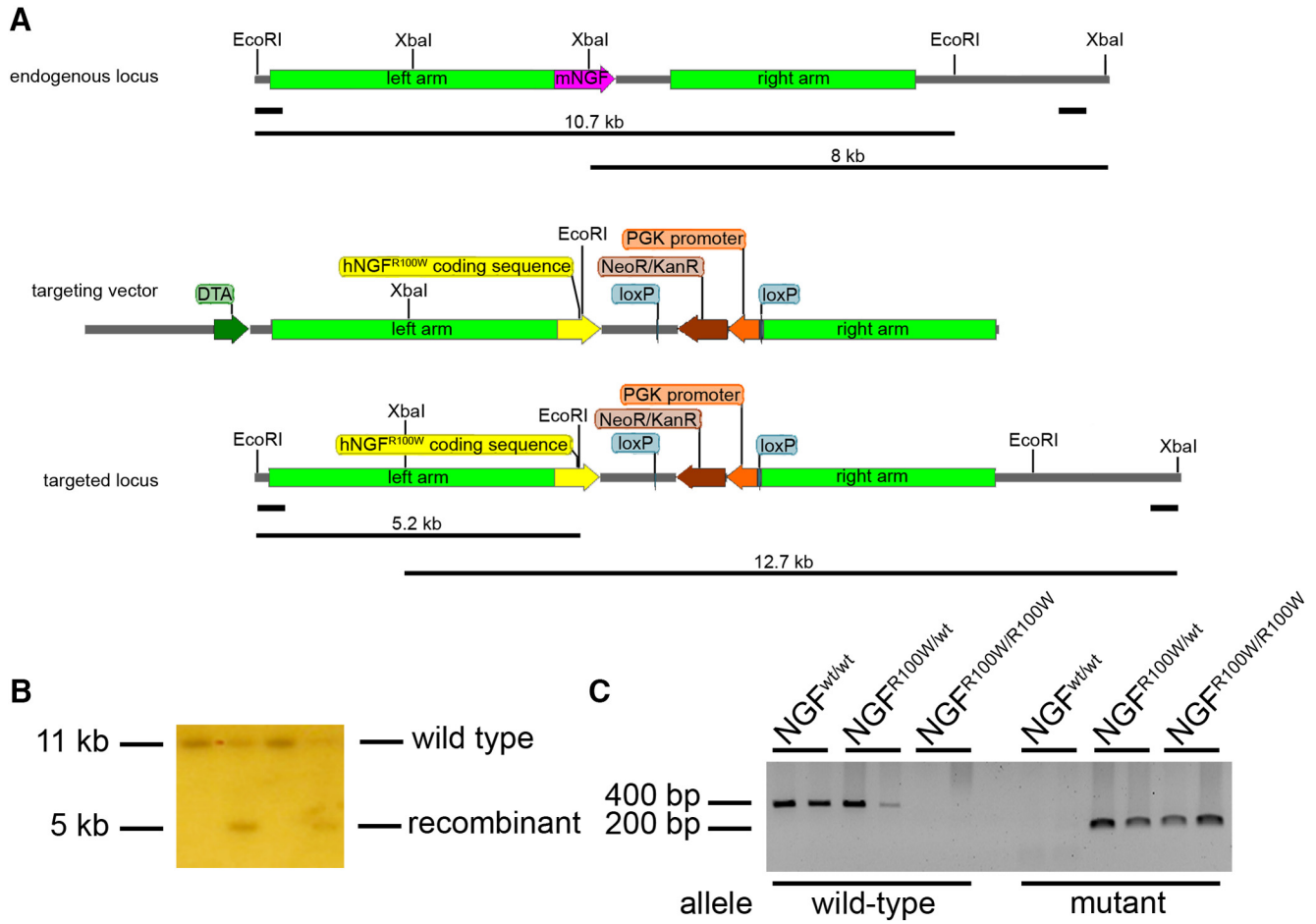


**Figure 1.** Molecular strategy for the generation of R100W knock-in mice. ***A***, *Top*, Endogenous mouse NGF locus with 5′ and 3′ Southern blot probes and expected sizes of wild-type Southern blot bands. *Middle*, Targeting vector for site-specific recombination. *Bottom*, Targeted NGF locus with 5′ and 3′ Southern blot probes and expected sizes of recombinant Southern Blot bands. Color codes are as follows: pink, mouse NGF coding sequence; yellow, human NGF coding sequence; brown, NeoR $^{+}$ selection cassette; orange, PGK promoter; blue, loxP sites; light green, left and right homology arms; dark green, DTA-negative selection marker. ***B***, Representative image of embryonic stem cells Southern blot. ***C***, PCR genotyping of NGF $^{R100W/wt}$, NGF $^{wt/wt}$, and NGF $^{R100W/R100W}$ mice; wild-type band, 400 bp; mutant band, 200 bp.

Positive clones were injected into C57BL/6 mouse blastocysts, and chimeric animals were obtained.

Mice were genotyped by PCR. The following PCR primers were used: fw_human: 5′-TTTAGCACCCAGCCTCCCCGTGAAG-3′; fw_mouse: 5′-CAGAAGGAGACTCTGTCCCTG-3′; and rev_human-mouse: 5′-CACCTCCTTGCCCTTGATGTCTG-3′.

Band sizes are as follows: wild-type, 400 bp; and mutant 200 bp (Fig. 1*C*).

*Behavioral analyses.* Experiments were performed on NGF $^{wt/wt}$, NGF $^{R100W/wt}$, mNGF $^{+/+}$, and mNGF $^{+/-}$ mice. Mice were kept under a 12 h light/dark cycle, with food and water available *ad libitum*.

*Hot plate test.* Mice were placed on a surface heated from 42°C to 54°C with 3°C steps. Animals were sequentially tested, allowing a 10 min resting period between each temperature step. The temperature threshold required to observe paw licking and the time required to observe this reaction at each temperature step were recorded.

*Cold sensitivity test.* Mice were put in a plastic cage and habituated for 30 min. Acetone (50 $\mu$l; Sigma-Aldrich) was sprayed onto the plantar surface of the hindpaw using a Gilson pipette, and the responses were reported as a 4-point score: 0 = no response; 1 = brisk withdrawal or flick of the paw; 2 = repeated flicking of paw; and 3 = repeated flicking of the hindpaw with licking. Acetone was applied six times, alternating between paws, with an interval of 5 min between each application. The frequency of response, expressed as a percentage (number of trial characterized by a response/total number of trials) was evaluated.

*Capsaicin injection test.* Mice were placed individually in a Plexiglas box for 15 min before drug injection to allow habituation. Capsaicin (catalog #141000, Abcam) was dissolved in dimethylsulfoxide (DMSO) and injected into the ventral surface of the right hindpaw using a Hamilton syringe at a concentration of 3 $\mu$g/$\mu$l in saline solution (total injection volume, 10 $\mu$l; DMSO final concentration, 0.1%). Control mice were injected with 10 $\mu$l of 0.1% DMSO in saline. Following the injection, mice were observed for 15 min and the amount of time spent licking and/or lifting the injected paw was measured.

*Object recognition test.* The apparatus consisted of a PVC arena (60 × 60 × 30 cm) with white floor and black walls. The test was performed in 3 d. On day 1, mice were subjected to a habituation phase in which they received two 5 min sessions in the empty arena, separated by a 30 min interval. On day 2, mice were exposed to two identical objects for 7 min to evaluate the total time of exploration. On day 3, mice were placed back in the arena and exposed to a familiar object and another novel object (memory phase). The time spent exploring each object was recorded.

*Morris water maze.* The test was performed in a water tank (120 cm diameter) filled with white opaque water. The platform, placed in the center of the southwest quadrant, was submerged 1 cm below the water surface. The 6-month-old mice were trained with two trials per day, with a 40 min interval, for 9 consecutive days. Mice were allowed up to 2 min to locate the platform, and the latency to reach it was recorded. If the mouse failed, the experimenter guided it onto the platform. Data were acquired and analyzed using an automated tracking system (Ethovision XT, Noldus).

*Tape response assay.* Mice were habituated to a Plexiglas container for 5 min, and then a 3 cm piece of adhesive tape was applied to the back. Mice were observed for 5 min to measure the latency to the first tape removal attempt and the total number of attempts.

*Cotton swab assay.* Mice were placed in an arena consisting of an elevated chamber with a grid floor and were allowed to habituate for 1 h. A cotton swab was stroked through the floor along the plantar paw surface five times, alternating between paws with a 10 s interval. The number of withdrawals was counted and expressed as a percentage of the total number of trials.

In vivo *nociceptive assay.* As reported in the study by Capsoni et al. (2011), CD1 male mice (Charles River, Italy) were subjected to a mechanical allodynia behavioral test after the injection of either WT or R100W NGF in the hindpaw plantar surface at a 0.2 $\mu$g/$\mu$l concentration (corresponding to 4 $\mu$g in a total injection volume of 20 $\mu$l) in saline. Control mice were injected with 20 $\mu$l of saline. The von Frey test (Ugo Basile, Italy) was performed before treatment and 1, 3, 4, and 5 h postinjection.

*NGF treatment.* Mouse wild-type NGF was administered daily at the dose of 1 $\mu$g/kg to pregnant dams by subcutaneous injection; treatment was protracted until 10 d after delivery. From postnatal day 10 (P10) to P60, pups received a daily subcutaneous injection (1 $\mu$g/kg) and intranasal administration (480 ng/kg) of NGF. A 21 d washout period was allowed before subsequent experiments.

*Dorsal root ganglion neuron primary cultures.* DRG neurons were prepared from neonatal (5-d-old, P5) Wistar rats (Charles River, Italy) from both sexes, as reported in the studies by Bonnington and McNaughton (2003) and Taneda et al. (2010). Briefly, DRGs were collected, incubated for 1 h at 37°C with 0.125% collagenase (Sigma-Aldrich), mechanically dissociated, and plated onto coverslips or Petri dishes pretreated with 10 $\mu$g/ml poly-L-lysine (Sigma-Aldrich), at a density of 50,000 cells/well of a 48-well tissue culture plate. DRG cultures were maintained in serum-free medium, consisting of DMEM/F12 (Invitrogen) supplemented with 87.5 ng/ml 5-fluoro-2′-deoxyuridine, 37.5 ng/ml uridine, 50 U/ml penicillin, and 50 $\mu$g/ml streptomycin (all from Sigma-Aldrich) and 0.05% Invitrogen N2 supplement (Thermo Fisher Scientific) at 37°C in 5% $CO_2$. The treatment with N2 supplement allows the presence of a physiological level of growth factors, thus preventing the occurrence of a neurotrophin withdrawal state. After 2–3 d *in vitro*, DRG cultures were stimulated for experimental procedures using either control human $NGF^{wt}$ or human $NGF^{R100W}$ (100 ng/ml) for 5 d or were maintained in basal medium conditions. At the end of this incubation period, B2R and phosphotransient receptor potential vanilloid-1 (pTRPV1) protein expression were measured by Western blot after 3 h of bradykinin (BK; 1 $\mu$M) application (antibodies used were as follows: rabbit anti-B2R, 1:1000, Alomone Labs; and rabbit anti-pTRPV1 and anti-TRPV1, both 1:1000, Millipore). Substance P (SP) was quantified in the culture medium using commercial enzyme immunoassay, according to the manufacturer instructions (Cayman Chemical).

To characterize neuronal viability, DRG cultures were fixed in 4% PFA for 10 min at room temperature (RT), incubated O/N at 4°C with mouse anti-NeuN (1:200; Sigma-Aldrich), and rabbit anti-Neurofilament 200 (1:200; Sigma-Aldrich) followed by goat anti-mouse secondary antibody (1:400; Sigma-Aldrich), goat anti-rabbit rhodamine-conjugated secondary antibody (1:1000; Sigma-Aldrich), and Hoechst 33258 (0.25 $\mu$g/ml) for 1 h and 5 min, respectively, at RT. Fluorescence images were acquired using an Olympus BX51 microscope and a 60× oil-immersion objective (numerical aperture, 1.4). The number of NeuN-immunoreactive cells was normalized on the total number of cells (i.e., Hoechst stained). At least 40 microscopic fields per coverslip, in four coverslips from three independent experiments, were quantified for each experimental group.

*Human $NGF^{R100W}$ purification.* Human $NGF^{R100W}$ cDNA was cloned into the prokaryotic expression vector pET19b downstream the sequence of the human BDNF prodomain, to produce a chimeric human proBDNF/$NGF^{R100W}$ construct, and expressed in the *Escherichia coli* strain Rosetta(DE3)PLysS. The corresponding chimeric protein was refolded from inclusion bodies and purified using an adaptation of the protocol used for proNGF in the study by Paoletti et al. (2015). The purified proBDNF-$NGF^{R100W}$ was proteolytically processed with trypsin to produce mature $NGF^{R100W}$, as previously described (Paoletti et al., 2015).

*Immunohistochemistry.* $NGF^{wt/wt}$, $NGF^{R100W/wt}$, $mNGF^{+/+}$, and $mNGF^{+/-}$ mice were transcardially perfused with 4% PFA in PBS, pH 7.4, and brains were dissected and postfixed O/N in the same solution, then cryoprotected in 30% sucrose in PBS for 36 h. The brains were sectioned with a sliding freezing microtome (Leica) to obtain 45-$\mu$m-thick coronal sections that were washed three times in TBS with 0.3% Triton X-100, then treated with 3.5% $H_2O_2$ in TBS to inactivate endogenous peroxidases. Sections were blocked for 30 min with 10% FBS and 0.3% Triton X-100 in TBS, followed by an O/N incubation at 4°C with 1:500 goat anti-choline acetyltransferase (ChAT; catalog #AB144P, Millipore). Biotinylated secondary antibodies (Vector Laboratories) were diluted in 10% FBS in PBS for 3 h at RT. Finally, sections were incubated in Vectastain ABC HRP Kit (Vector Laboratories) in PBS for 1 h, followed by another incubation in TBS solution containing diaminobenzidine (DAB; Sigma-Aldrich) and the enzyme Glucose Oxidase type VII (Sigma-Aldrich); the reaction was stopped after 10 min. Stained sections were mounted on glass slides using DPX Medium. Images were acquired with a Nikon Eclipse E600 Optical Microscope, and the density of immunoreactive cells was calculated using ImageJ.

For analysis of superior cervical ganglia (SCGs), embryonic day 16.5 fetuses were extracted from pregnant dams, washed in PBS, and fixed by immersion in 4% PFA for 4 h, then cryoprotected in 30% sucrose in PBS and sectioned using a cryostat. The quantification of SCG cell number was performed on Nissl-stained sections, with the experimenter blind to the genotype of the animal, and representative images were obtained by staining for tyrosine hydroxylase (TH; 1:200; catalog #AB152, Millipore) O/N at 4°C (Crerar et al., 2019); subsequent steps were as described above.

Whole-mount staining was performed on internal organs dissected from P0.5 pups, O/N fixed in 4% PFA, then dehydrated in methanol series, followed by O/N quenching of endogenous peroxidases in 80% methanol, 17% DMSO, and 3% $H_2O_2$. After rehydration, samples were blocked in 4% BSA, 1% Triton X-100 in PBS, and incubated with 1:200 anti-TH antibody diluted in the same blocking solution for 72 h at 4°C. The signal was revealed by incubation with HRP-conjugated anti-rabbit antibody (1:200; catalog #sc-2004, Santa Cruz Biotechnology) diluted in blocking solution O/N at 4°C, followed by DAB processing. Finally, samples were cleared using a 2:1 solution of benzyl benzoate and benzyl alcohol (Crerar et al., 2019). Samples were imaged using a 4× objective, and optical density of the signal was quantified with the experimenter blind to the genotype of the animal.

*Skin and DRG immunofluorescence.* DRGs from adult mice (2 and 6 months old) were collected in an Eppendorf tube containing cold PBS, then postfixed in 4% PFA for 30 min at RT, embedded in 2% agarose and sectioned at 50 $\mu$m thickness using a vibratome. Sections were washed twice with PBS-Triton 0.3%, then subjected to a 30 min blocking step in 5% NGS and 0.3% Triton X-100 in PBS, followed by an O/N incubation at 4°C with primary antibodies diluted as shown below. Alexa Fluor-conjugated secondary antibodies (Thermo Fisher Scientific) were diluted 1:1000 in 0.3% Triton X-100 and 5% NGS in PBS for 2 h at RT. Sections were mounted using Invitrogen Prolong Gold Medium (Thermo Fisher Scientific).

For immunofluorescence analysis, the hairy and glabrous skins were collected, allowed to dry, and postfixed in 4% PFA at 4°C O/N, then incubated in 30% sucrose in PBS and frozen in OCT (optimal cutting temperature) medium (Leica). Sections (50 $\mu$m thick for hairy skin, 20 $\mu$m thick for glabrous skin) were obtained using a cryostat. Immunostaining was performed as described above.

The antibodies and dilutions used were as follows: 1:500 mouse anti-NF200 (Sigma-Aldrich); 1:200 mouse anti-calcitonin gene-related peptide (CGRP; Rockland); 1:100 Invitrogen isolectin GS-B4-biotin conjugate (Thermo Fisher Scientific); 1:200 rabbit anti-B2R (Alomone Labs); 1:300 mouse anti-TRPV1 (Millipore); 1:200 Dako rabbit anti-PGP 9.5 (Agilent Technologies); and 1:300 rabbit anti-NGF M20 (Santa Cruz Biotechnology).

The M20 anti-NGF antibody was validated by measuring the immunofluorescence signal intensity obtained using different dilutions on glabrous skin samples from $NGF^{+/+}$ and $NGF^{+/-}$ mice. A nonlimiting concentration of the primary antibody (0.67 $\mu$g/ml) was able to detect the lower skin NGF content in $NGF^{+/-}$ mice compared with $NGF^{+/+}$ mice. Decreasing the antibody concentration (0.33 $\mu$g/ml) led to incom-

plete titration of NGF in the skin of NGF$^{+/+}$ mice, whereas the signal in samples from NGF$^{+/-}$ mice was unaffected. Further dilution of the antibody (0.17 $\mu$g/ml) resulted in inefficient detection of NGF in samples from both NGF$^{+/+}$ and NGF$^{+/-}$ mice. ANOVA-2 (antibody concentration $\times$ genotype interaction, $F_{(2,34)} = 3.563$, $p = 0.039$) followed by Holm–Sidak *post hoc* test (0.67 $\mu$g/ml; NGF$^{+/+}$ vs NGF$^{+/-}$, $p < 0.001$; 0.33 $\mu$g/ml; NGF$^{+/+}$ vs NGF$^{+/-}$, $p < 0.001$, 0.17 $\mu$g/ml; NGF$^{+/+}$ vs NGF$^{+/-}$, $p = 0.314$; NGF$^{+/+}$: 0.67 vs 0.33 $\mu$g/ml, $p = 0.303$; 0.67 vs 0.17 $\mu$g/ml, $p < 0.001$; 0.33 vs 0.17 $\mu$g/ml, $p < 0.001$; NGF$^{+/-}$: 0.67 vs 0.33 $\mu$g/ml, $p = 0.697$; 0.67 vs 0.17 $\mu$g/ml, $p = 0.047$; 0.33 vs 0.17 $\mu$g/ml, $p = 0.030$; $n = 7$ for each group).

All images were acquired with a Leica SP5 Confocal Microscope and analyzed with Fiji (NIH).

*RNA preparation for microarray analysis.* DRGs from wild-type and NGF$^{R100W/wt}$ mice (6 months of age) were isolated and collected. The total RNA was extracted with TRIzol reagent (Life Technologies) according to the manufacturer instructions, DNase treated, and purified using Qiagen columns. RNA content was determined on a NanoDrop UV-VIS Spectrophotometer. Only samples with an absorbance ratio of $1.8 < OD_{260}/OD_{280} < 2.0$ were further processed. Each sample was then quality checked for integrity using a BioAnalyzer 2100 (RNA 6000 Nano Kit, catalog #G2938C, Agilent Technologies).

*Whole-genome expression profiling.* Gene expression profiling was performed using the Agilent Technologies one-color microarray system. Two hundred nanograms of Poly A+RNA were retrotranscribed using oligo-dT primers linked to the T7 promoter, and the resulting cDNA was used as a template for cyanine 3-CTP (cytidine triphosphate)-labeled cRNA preparation, using the Agilent Technologies Low Input Linear Amplification Kit. The labeled cRNA was purified with RNeasy Mini Spin Columns (Qiagen). To monitor both the labeling reactions and the microarray performance, Agilent Technologies Spike-In Mix was added to the mRNA samples before labeling reactions according the RNA Spike-In protocol. Cyanine 3-labeled cRNA was hybridized to Agilent Technologies 8x60K whole-mouse genome oligonucleotide microarrays (Grid ID, 028005). Microarray hybridizations were performed in SureHyb Hybridization Chambers (Agilent Technologies) containing 600 ng of cyanine 3-labeled cRNA per hybridization. The hybridization reactions were performed at 65°C for 17 h using the Gene Expression Hybridization Kit (Agilent Technologies). The hybridized microarrays were disassembled at RT in Gene Expression Wash Buffer 1 (Agilent Technologies). After disassembly, the microarrays were washed in Gene Expression Wash Buffer 1 for 1 min at RT, followed by washing with Gene Expression Wash Buffer 2 for 1 min at 37°C. Then, microarrays were treated with acetonitrile for 1 min at RT. Fluorescence signals of the hybridized Agilent Technologies Microarrays were detected using the Microarray Scanner System (catalog #G2564B, Agilent Technologies). The Feature Extraction Software (version 10.7.3.1, Agilent Technologies) was used to process the microarray image files.

*Microarray data analysis.* Data filtering, normalization, analysis, and plotting were performed using R-Bioconductor (https://www.bioconductor.org/). In particular, differential expression was analyzed with the R package limma version 3.5 (Ritchie et al., 2015). All the features with the flag gIsWellAboveBG = 0 (too close to background) were filtered out and excluded from the following analysis. Filtered data were normalized by aligning samples to the 75th percentile. Differentially expressed genes were selected by a combination of fold-change and moderated *t* test thresholds (R limma test with FDR < 0.05; |Log2 fold change ratio| > 1.0). Pathway analysis and network plotting of differential gene lists was performed using the on-line tool StringDB (https://string-db.org; (Szklarczyk et al., 2015).

*Electron microscopy.* Fixed nerves were washed in phosphate buffer at RT (10 $\times$ 5 min), osmicated in 2% (w/v) $OsO_4$ in $H_2O$ (2 h at 4°C), washed again (0.05 M maleate buffer, pH 5.15–10 $\times$ 5 min), then dehydrated in ethanol (70%, v/v) for 15 min; 80% (v/v) for 15 min; 90% (v/v) for 15 min; 100%, 4 $\times$ 15 min). Subsequently, nerves were infiltrated first with propylene-oxide (2 $\times$ 15 min) then with a mixture of 50% (v/v) propylene-oxide and 50% (v/v) resin catalyzed with 2% DMP30 overnight at RT. Embedding (100% resin catalyzed with 2% DMP30) was followed by 24 h heat treatment for proper polymerization of resin at 65°C. Myelinated axons were counted on semithin (1-$\mu$m-thick) sections stained with toluidine blue and imaged with a Zeiss Axioplan light microscope. Myelinated fibers were counted individually using MetaMorph software (Molecular Devices). In cases of multiple nerve components (i.e., separate bundles of fibers, with individual connective sheets), fiber counts were performed for each component and the corresponding values were summed up. Unmyelinated axons were counted with the aid of transmission electron microscopy at 20,000$\times$ magnification. Sectioning was performed using a Leica Ultracut Ultramicrotome. Ultrathin sections (90 nm thick) were collected on single-hole copper grids (Formvar Support Film Slots, 2 $\times$ 1 mm Cu grids; FF2010-CU). Images were obtained using a Jeol 1200EX II Transmission Electron Microscope equipped with a charge-coupled device Olympus Veleta Megaview camera covering 5% of the total cross-sectional area of the nerve. Based on the cross-sectional area, a total of 211 fields/NGF$^{wt/wt}$ and 146 fields/NGF$^{R100W/wt}$ samples were obtained covering central as well as peripheral portions of each nerve systematically. Image files were saved as a TIFF and transferred to MetaMorph, where axons were counted manually.

*Nerve conduction velocity measurements.* Mice were killed using $CO_2$ inhalation, and the saphenous nerve was dissected and placed in an organ bath (Wetzel et al., 2007). The chamber was perfused with a synthetic interstitial fluid buffer containing the following (in mM): NaCl 123, KCl 3.5, $MgSO_4$ 0.7, $NaH_2PO_4$ 1.7, $CaCl_2$ 2.0, Na-gluconate 9.5, glucose 5.5, sucrose 7.5, and HEPES 10, pH 7.4, at 3 ml/min at 32°C. The distal part of the nerve was placed in the organ bath, while the proximal part was placed in an adjacent chamber filled with mineral oil for recording. An electric probe was used to stimulate the nerve, and a compound action potential was recorded and analyzed using LabChart4 software (AD Instruments, Australia). Each electrical stimulus elicited a response consisting of three peaks, corresponding to the A$\beta$, A$\delta$, and C fibers, respectively. To measure the conduction velocity of each fiber type, the distance between the electric probe and the recording electrode was divided by the time elapsed from the beginning of the stimulus to the appearance of the peak.

*Electrophysiology on brain slices.* Acute brain slices were prepared from 5- to 6-month-old mice, following the protocol described in the study by Barone et al. (2018). Mice were killed by cervical dislocation, and the brain was quickly dissected in an ice-cold, $O_2$-saturated cutting solution containing the following (in mM[SCAP]): NaCl 85, sucrose 75, glucose 25, $NaHCO_3$ 24, KCl $MgCl_2$ 4, 2.5, $NaHPO_4$ 1.25, and $CaCl_2$ 0.5, pH 7.4. The 350-$\mu$m-thick sections were prepared using a Leica VT-1200S vibratome while keeping the brain immersed in the same ice-cold cutting solution. Sections were transferred to a recovery chamber filled with artificial CSF (aCSF) containing the following (in mM): NaCl 119, glucose 10, HEPES 10, $NaHCO_3$ 6.2, KCl 2.5, $CaCl_2$ 2, $MgCl_2$ 1.2, and $NaH_2PO_4$ 1, pH 7.4, and was held at 32°C for 30 min, then recovery was completed for an additional 60 min at RT. For recording, sections were transferred to a submerged chamber continuously perfused with aCSF at 32°C saturated with $O_2$, and a concentric bipolar stimulating electrode was used to stimulate Schaffer collateral pathway fibers, while a glass pipette (1 M$\Omega$ impedance) filled with aCSF was placed in the CA1 stratum radiatum. Field EPSPs (fEPSPs) were recorded using a MultiClamp 700A Amplifier plugged to a Digidata 1322A interface (Molecular Devices). Current stimuli were delivered using a stimulus isolator (WPI). By using a stimulus intensity eliciting a response that amounted to 30–50% of the maximum, a stable baseline, using a 0.05 Hz test stimulus frequency, was obtained before delivering high-frequency stimulation (HFS; four trains of 1 s at 100 Hz, with an intertrain interval of 10 s) to induce long-term potentiation. The post-HFS fEPSP was monitored for at least 60 min. Data were analyzed using Clampfit (Molecular Devices). The experimenter was blind to the genotype of the animal.

*Hek293 cells culture.* Hek293 cells were maintained at 37°C, 5% $CO_2$, in Gibco DMEM/F-12 medium supplemented with 10% FBS, 1% L-glutamine, and 1% penicillin/streptomycin (Thermo Fisher Scientific). Hek293 cells were transfected with pCMV6-XL5-human NGF$^{wt}$ and pCMV6-XL5-human NGF$^{R100W}$ plasmids following the manufacturer instructions for Invitrogen Lipofectamine 2000 (Thermo Fisher Scientific). Forty-eight hours after transfection, the supernatants were immu-

noprecipitated and subjected to Western blotting as described below (see NGF immunoprecipitation and Western blot).

*NGF immunoprecipitation and Western blot.* Cerebral cortices were isolated from adult mice and homogenized in lysis buffer (Tris-HCl 100 mM, NaCl 400 mM, SDS 0.1%, and Triton X-100 1%). The homogenates were sonicated, incubated in ice for 30 min, and centrifuged at 15,000 × *g* for 30 min at 4°C. Protein concentration in the supernatant was quantified using the Bradford method (Bio-Rad). Four milligrams of protein were immunoprecipitated with an excess of anti-NGF αD11 antibody in NET Gel Buffer (Tris-HCl, pH 7.5, 50 mM; NaCl 150 mM; 0.1% Nonidet P-40; EDTA, pH 8, 1 mM; 0.25% gelatin; and 0.02% NaN). After immunoprecipitation, total lysates were loaded on 12% acrylamide gels and blotted using nitrocellulose membranes. The primary antibody was anti-NGF M20 (1:500; Santa Cruz Biotechnology), the secondary antibody was goat anti-rabbit HRP-conjugated (1:500; Santa Cruz Biotechnology). Blot images were acquired using a ChemiDoc System (Bio-Rad), and the optical density was quantified using ImageJ (NIH).

*Data analysis and statistics.* Statistical significance was assessed using SigmaStat 12 (Systat Software). Data are presented as the mean ± SEM; detailed statistics for every comparison are reported in the corresponding figure legend.

## Results

### Generation of NGF$^{R100W/wt}$ mice and characterization of their nociceptive phenotype

To shed light on the consequences of the HSAN V-associated NGF$^{R100W}$ mutation, we generated a knock-in mouse line harboring the human *NGF$^{R100W}$* sequence (Fig. 1). Homozygous NGF$^{R100W/R100W}$ mice die by P30; Testa et al., 2019). On the other hand, heterozygous mice thrive normally and show no visible gross deficit. We analyzed the phenotype of heterozygous NGF$^{R100W/wt}$ mice in detail, during youth (2 months) and adulthood (6 months). Chemical nociception induced by capsaicin injection in the hindpaw was impaired at both ages (Fig. 2*A*). Thermal nociception was normal at 2 months of age and decreased at 6 months, with adult NGF$^{R100W/wt}$ mice displaying a higher latency to respond to a high-temperature stimulus (Fig. 2*B*). On the other hand, cold sensitivity, measured by topical acetone application on the hindpaw was reduced at both ages (Fig. 2*C*). In NGF$^{R100W/wt}$ mice, a non-noxious stimulus represented by a small piece of tape applied to the back (i.e., to the hairy skin) took more time to induce a removal reaction only at 6 months of age (Fig. 2*D*). On the other hand, the response to gentle stroking of the glabrous skin was normal at both time points (Fig. 2*E*).

These behavioral data show that NGF$^{R100W/wt}$ mice have a reduced responsiveness to chemical and thermal noxious stimuli, are less sensitive to somatosensory inputs, but display normal light touch.

### Phenotypic analysis of DRGs from NGF$^{R100W/wt}$ mice

To look for a cellular-functional correlate of the impaired nociceptive behavior of NGF$^{R100W/wt}$ mice, we first focused on the two main NGF-sensitive neuronal populations, defined by the expression of IB4 and CGRP, respectively (Harrison et al., 2004). We imaged DRGs from 2- and 6-month-old NGF$^{R100W/wt}$ mice and found no change in the total number of DRG neurons (2 months: NGF$^{R100W/wt}$, 1040.4 ± 37.9 cells/mm$^2$; NGF$^{wt/wt}$, 1003.3 ± 52.7 cells/mm$^2$; $n = 3$/group; Student's *t* test, $p = 0.598$, $t = -0.571$; 6 months: NGF$^{R100W/wt}$, 1340.4 ± 36.8 cells/mm$^2$; NGF$^{wt/wt}$, 1391.1 ± 29.5 cells/mm$^2$; Student's *t* test, $p = 0.324$, $t = 1.044$; NGF$^{R100W/wt}$, $n = 6$; NGF$^{wt/wt}$, $n = 5$) and in the percentages of cells expressing the neurofilament marker NF200, the nonpeptidergic nociceptor marker IB4, and the peptidergic nociceptor marker CGRP, respectively (Fig. 3*A*). We also analyzed DRGs from P5 mice, an early postnatal developmental stage during which segregation between peptidergic and nonpeptidergic neurons is in progress (Molliver et al., 1997) and found no differences between NGF$^{R100W/wt}$ mice and controls in the total cell number (NGF$^{R100W/wt}$, 2134.3 ± 64.6 cells/mm$^2$; NGF$^{wt/wt}$, 2234.2 ± 116.9 cells/mm$^2$; $n = 5$ and $n = 4$, respectively; Student's *t* test, $p = 0.454$, $t = 0.793$) or in the percentages of either NF200$^+$, IB4$^+$, or CGRP$^+$ cells (Fig. 3*B*). This suggests that the neurotrophic potency of NGF$^{R100W}$ on DRG neurons is comparable to NGF$^{wt}$. This was also demonstrated in an *in vitro* DRG neuron survival assay (NGF$^{R100W}$, 158.2 ± 8.8%; NGF$^{wt}$, 162.3 ± 18.03%; control, 100.0 ± 5.0% NeuN$^+$/total Hoechst$^+$ cells; ANOVA-1, $F_{(2,17)} = 8.621$, $p = 0.003$; followed by Bonferroni *post hoc* test: NGF$^{R100W}$ vs NGF$^{wt}$, $p = 1.000$; NGF$^{wt}$ vs control, $p = 0.006$; NGF$^{R100W}$ vs control, $p = 0.01$; $n = 6$ for each group). Given that the sympathetic nervous system is highly dependent on an intact NGF function for proper development (Levi-Montalcini and Booker, 1960; Glebova and Ginty, 2004), the unaltered neurotrophic actions of NGF$^{R100W}$ are also supported by the normal cell number of the SCG (Fig. 3*C*) and by the normal sympathetic innervation of key target organs (i.e., heart, stomach, kidney, spleen), as revealed by TH immunohistochemistry (Fig. 3*D*).

However, when we analyzed BK receptor 2 (B2R), whose expression is upregulated by NGF (Petersen et al., 1998), and TRPV1, an NGF-responsive detector of heat- and capsaicin-induced pain (Zhang et al., 2005), we found a significantly decreased immunoreactivity for both receptors (Fig. 3*E*).

To detect subtler changes in DRGs from NGF$^{R100W/wt}$ mice, we performed a transcriptomic analysis to identify differentially expressed genes with respect to DRGs from wild-type mice. The data showed only a small number of differentially expressed genes in DRGs from NGF$^{R100W/wt}$ versus wild-type mice (Fig. 3*F* and Fig. 3-1, available at https://doi.org/10.1523/JNEUROSCI.0688-19.2019.f3-1), which is in line with the globally normal appearance of DRG neuronal subpopulations. Among the regulated genes, TyroBP (*DAP12*) and toll-like receptor 2 (*TLR2*) are noteworthy for their involvement in glial function (Liu et al., 2012; Shboul et al., 2019). Indeed, gene ontology and network analysis of differentially expressed genes in DRGs revealed that the R100W mutation significantly affects pathways involved in immune response, phagocytosis and Rho GTPase cycle (Fig. 3*G*), suggesting a major effect of the R100W mutation on DRG glial and microglial cells, rather than on DRG neurons.

These findings demonstrate that DRG neurons from NGF$^{R100W/wt}$ mice show only specific molecular changes directly linked to nociception, alongside an intriguing modulation of glia-related genes.

### Pain sensitization by NGF$^{R100W}$ protein

To investigate whether the R100W mutation might also affect DRG function, we explored the ability of the NGF$^{R100W}$ protein to activate and sensitize wild-type DRGs. Incubation of DRG neuronal cultures with NGF$^{R100W}$, followed by acute administration of the inflammatory neuropeptide BK (Chuang et al., 2001), led to reduced SP release (Fig. 4*A*), bradykinin B2R receptor expression (Fig. 4*B*), and TRPV1 phosphorylation (Fig. 4*C*), respectively. The reduced ability of NGF$^{R100W}$ to sensitize neurons *in vitro* was paralleled by *in vivo* experiments, using acute injection of NGF$^{R100W}$ in the hindpaw of CD1 mice. This treatment resulted in a significantly lower mechanical allodynia with respect to mice injected with NGF$^{wt}$ (Fig. 4*D*). Thus, NGF$^{R100W}$ dimin-

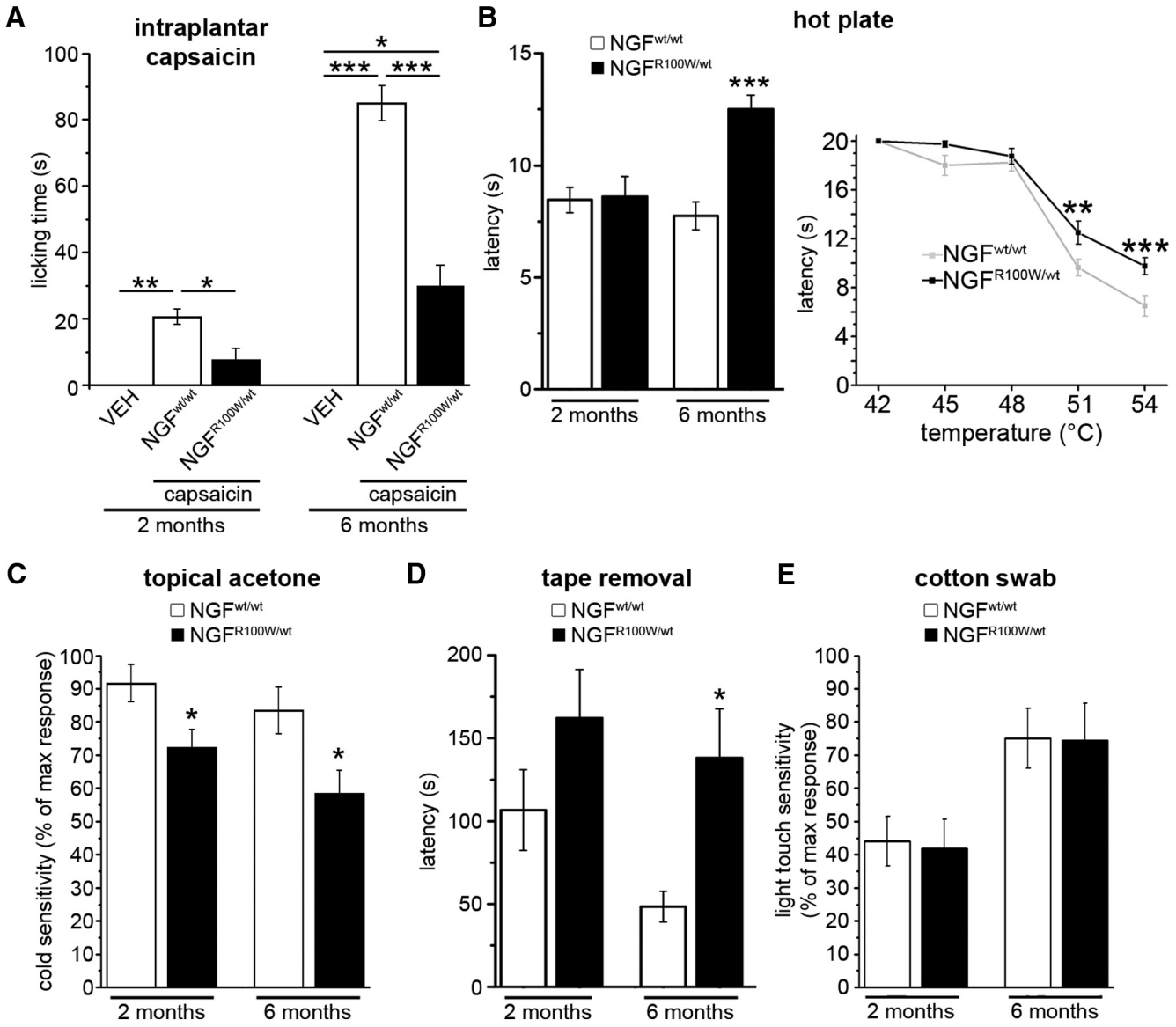


**Figure 2.** The R100W mutation is associated with decreased sensitivity to noxious stimuli. ***A***, Decreased hyperalgesic response to capsaicin in juveniles and adults. Two months, ANOVA-1 ($F_{(2,12)} = 12.869$, $p = 0.002$), followed by Bonferroni *post hoc* test (NGF$^{wt/wt}$ vs VEH, $^{**}p = 0.002$; NGF$^{wt/wt}$ vs NGF$^{R100W/wt}$, $^{*}p = 0.017$; NGF$^{R100W/wt}$ vs VEH, n.s.); VEH, $n = 3$; NGF$^{wt/wt}$, $n = 5$; NGF$^{R100W/wt}$, $n = 5$. 6 months, ANOVA-1 ($F_{(2,13)} = 49.995$, $p < 0.001$), followed by Bonferroni *post hoc* test (NGF$^{wt/wt}$ vs VEH, $^{***}p < 0.001$; NGF$^{wt/wt}$ vs NGF$^{R100W/wt}$, $^{***}p < 0.001$; NGF$^{R100W/wt}$ vs VEH, $p = 0.017$); VEH, $n = 3$; NGF$^{wt/wt}$, $n = 5$; NGF$^{R100W/wt}$, $n = 6$. ***B***, Normal sensitivity to hot stimuli at 2 months of age and impairment in adult HSAN V mice, with increased latency in NGF$^{R100W/wt}$ animals to respond to high temperatures. *Left*, 2 months, Student's two-tailed *t* test ($t = 0.126$, $p = 0.901$); NGF$^{wt/wt}$, $n = 11$; NGF$^{R100W/wt}$, $n = 15$. 6 months, Student's two-tailed *t* test ($t = 4.743$, $p < 0.001$); NGF$^{wt/wt}$, $n = 4$; NGF$^{R100W/wt}$, $n = 9$. *Right*, ANOVA-2 ("genotype" × "temperature" interaction, $F_{(4,79)} = 3.283$, $p = 0.017$), followed by Bonferroni *post hoc* test, $^{***}p < 0.001$, $^{**}p = 0.003$; NGF$^{wt/wt}$, $n = 8$; NGF$^{R100W/wt}$, $n = 8$. ***C***, Impaired cold sensitivity in both juveniles and adults. 2 months, Student's two-tailed *t* test ($t = 2.445$, $^{*}p = 0.035$); NGF$^{wt/wt}$, $n = 6$; NGF$^{R100W/wt}$, $n = 6$. 6 months, Student's two-tailed *t* test ($t = 2.457$, $^{*}p = 0.026$); NGF$^{wt/wt}$, $n = 8$; NGF$^{R100W/wt}$, $n = 10$. ***D***, Decreased hairy skin sensitivity in adult HSAN V mice. 2 months, Student's two-tailed *t* test ($t = 1.261$, $p = 0.226$); NGF$^{wt/wt}$, $n = 6$; NGF$^{R100W/wt}$, $n = 11$. 6 months, Student's two-tailed *t* test ($t = 2.305$, $^{*}p = 0.042$); NGF$^{wt/wt}$, $n = 5$; NGF$^{R100W/wt}$, $n = 8$. ***E***, Normal light touch sensitivity. 2 months, Student's two-tailed *t* test ($t = 0.155$, $p = 0.879$); NGF$^{wt/wt}$, $n = 5$; NGF$^{R100W/wt}$, $n = 11$. 6 months, Student's two-tailed *t* test ($t = 0.050$, $p = 0.961$); NGF$^{wt/wt}$, $n = 8$; NGF$^{R100W/wt}$, $n = 7$.

ishes the propensity of DRGs to sensitize and to increase transmission of noxious stimuli.

### Exploring nociceptive information routes in NGF$^{R100W/wt}$ mice

The above-described *in vitro* and *in vivo* results prompted us to analyze the nociceptive input path. We first ruled out that the observed behavioral effects (Fig. 2) were due to a nerve conduction deficit; indeed, the conduction velocities of the three main sensory fiber populations, Aβ, Aδ and C fibers, were normal (Fig. 5*A*).

We then analyzed the ultrastructure of the sciatic nerve using transmission electron microscopy. Compared with controls, the cross-sectional area of the whole nerve in NGF$^{R100W/wt}$ mice was significantly decreased (Fig. 5*B*). In this regard, the number of myelinated axons contained in the nerve was unaffected, whereas a significant decrease in the number of nonmyelinated axons in NGF$^{R100W/wt}$ mice was observed (Fig. 5*B*), which might determine the smaller overall nerve section. These neurophysiological and ultrastructural data match analogous findings in HSAN V heterozygous human carriers (Minde et al., 2009).

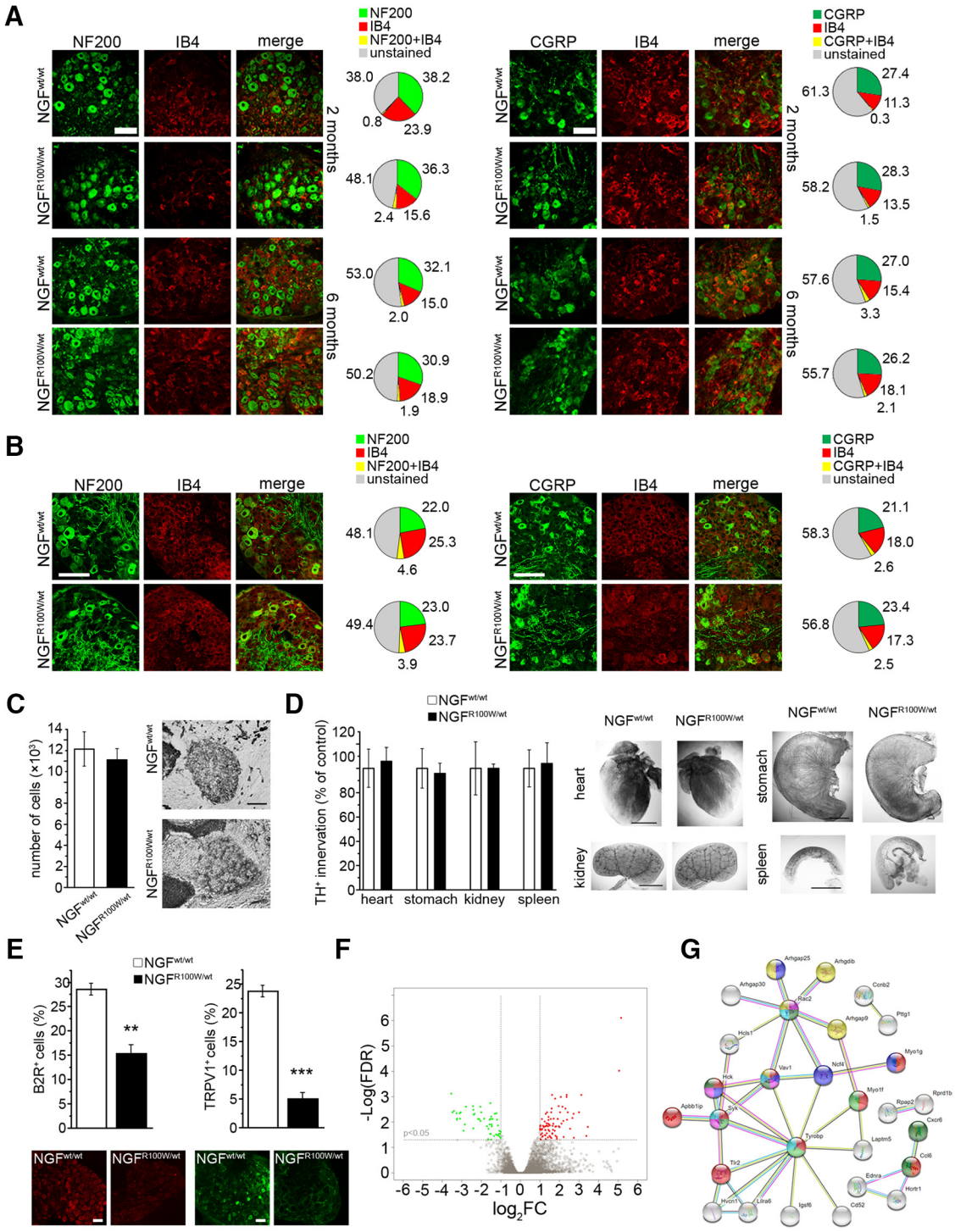


**Figure 3.** Analysis of DRG markers, sympathetic neurons and innervation, and DRG transcriptome of NGF$^{R100W/wt}$ mice. ***A***, ***B***, Normal expression of NF200, IB4, and CGRP in DRG neurons in both juveniles and adults (***A***) and in P5 mice (***B***). Scale bars, 100 $\mu$m. ***C***, No significant difference in SCG cell numbers from NGF$^{R100W/wt}$ and NGF$^{wt/wt}$ mice; Student's two-tailed *t* test: $t = 0.482$, $p = 0.650$; NGF$^{wt/wt}$, $n = 4$; NGF$^{R100W/wt}$, $n = 3$. Scale bar, 100 $\mu$m. ***D***, Normal sympathetic innervation of target internal organs in NGF$^{R100W/wt}$ mice with respect to NGF$^{wt/wt}$ controls; heart, Student's two-tailed *t* test: $t = -0.268$, $p = 0.796$; NGF$^{wt/wt}$, $n = 6$; NGF$^{R100W/wt}$, $n = 4$; stomach, Student's two-tailed *t* test: $t = 0.216$, $p = 0.835$; NGF$^{wt/wt}$, $n = 5$; NGF$^{R100W/wt}$, $n = 4$; kidney, Student's two-tailed *t* test: $t = -0.002$, $p = 0.999$; NGF$^{wt/wt}$, $n = 6$; NGF$^{R100W/wt}$, $n = 4$; spleen, Student's two-tailed *t* test: $t = -0.165$, $p = 0.874$; NGF$^{wt/wt}$, $n = 5$; NGF$^{R100W/wt}$, $n = 3$. Scale bars, 1 mm. ***E***, Reduced expression of B2R and TRPV1 in DRG neurons of adult mice. Scale bar, 50 $\mu$m. B2R, Student's two-tailed *t* test: $t = 6.219$, $^{**}p = 0.003$; NGF$^{wt/wt}$, $n = 3$; NGF$^{R100W/wt}$, $n = 3$. TRPV1, Student's two-tailed *t* test: $t = 12.455$, $^{***}p < 0.001$; NGF$^{wt/wt}$, $n = 4$; NGF$^{R100W/wt}$, $n = 4$. ***F***, Volcano plot for differentially expressed genes in DRGs. The *x*-axis corresponds to log$_2$FC (Log$_2$FoldChange) differential expression, and the *y*-axis to −Log(FDR; −Log false discovery rate corrected *p* value). Red and green regions show significantly upregulated and downregulated genes, respectively. The log$_2$FC and −Log(FDR) thresholds are shown as horizontal (−Log(FDR)<0.05) and vertical (|log$_2$FC|>2.0) dashed lines (see Figure 3-1, available at https://doi.org/10.1523/JNEUROSCI.0688-19.2019.f3-1). ***G***, Pathway analysis of differentially expressed genes in DRGs. The gene–gene network was obtained by StringDB tool (https://string-db.org). Colors indicate genes belonging to the main over-represented pathways and functional categories: immune response and chemokines (red and green), phagocytosis (blue and purple), killer cells mediated cytotoxicity (light blue), and rho GTPase (yellow).

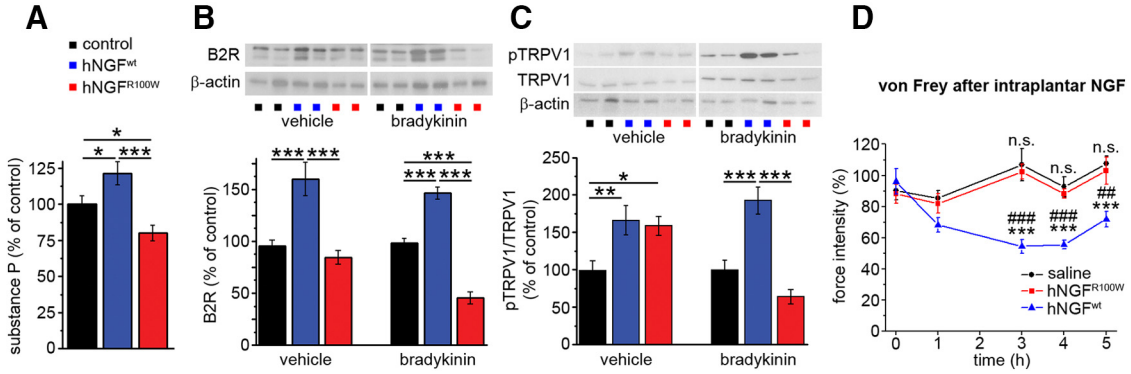


**Figure 4.** Reduced *in vitro* and *in vivo* sensitization capability of NGF$^{R100W}$. ***A***, Bradykinin-induced SP release in DRG cultures is reduced by NGF$^{R100W}$ cotreatment compared with NGF$^{wt}$. ANOVA-1 ($F_{(2,16)} = 10.501$, $p < 0.002$) followed by Student–Newman–Keuls *post hoc* test, ***$p < 0.001$, *$p = 0.03$; hNGF$^{wt}$, $n = 5$; hNGF$^{R100W}$, $n = 6$; control, $n = 6$. ***B***, Downregulation of B2R expression by NGF$^{R100W}$ in DRG cultures stimulated with bradykinin. ANOVA-2 (NGF × bradykinin interaction, $F_{(2,45)} = 3.371$, $p = 0.044$) followed by Bonferroni *post hoc* test, ***$p < 0.001$; hNGF$^{wt}$-vehicle, $n = 7$; hNGF$^{R100W}$-vehicle, $n = 8$; control-vehicle, $n = 8$; hNGF$^{wt}$-bradykinin, $n = 8$; hNGF$^{R100W}$-bradykinin, $n = 7$; control-bradykinin, $n = 8$. ***C***, Reduced phosphorylation of TRPV1 by NGF$^{R100W}$ in DRG cultures stimulated with bradykinin. ANOVA-2 (NGF × bradykinin interaction, $F_{(2,47)} = 9.346$, $p < 0.001$) followed by Bonferroni *post hoc* test, ***$p < 0.001$, **$p = 0.008$, *$p = 0.02$; $n = 8$ for each group. ***D***, Human NGF$^{R100W}$ intraplantar injection causes reduced mechanical sensitization compared with human NGF$^{wt}$. ANOVA-2 repeated-measures test (treatment × time interaction, $F_{(8,144)} = 5.785$, $p < 0.001$) followed by Bonferroni *post hoc* test, hNGF$^{wt}$ versus saline, ***$p < 0.001$; hNGF$^{wt}$ versus hNGF$^{R100W}$, ###$p < 0.001$, ##$p = 0.002$, hNGF$^{R100W}$ vs saline, n.s. $p = 1.000$; saline, $n = 10$; hNGF$^{wt}$, $n = 11$; hNGF$^{R100W}$, $n = 9$.

Finally, we analyzed target tissues of sensory fibers, namely hairy and glabrous skin (Zimmerman et al., 2014). The area of PGP9.5-immunoreactive terminals was not significantly different at 2 months of age, whereas, at 6 months of age, NGF$^{R100W/wt}$ mice showed a significant reduction in both hairy and glabrous skin sensory innervation (Fig. 5*C*,*D*). This is in keeping with the reduction in the skin innervation of individuals with HSAN V (Axelsson et al., 2009). Moreover, the age-dependent decrease in PGP9.5-immunoreactive fibers in the hairy skin correlates with the lower performance of NGF$^{R100W/wt}$ mice in the tape removal test (Fig. 2*D*).

Since target-derived NGF modulates innervation (Davies et al., 1987; Purves et al., 1988), we analyzed NGF expression in the glabrous skin by immunofluorescence and found a significantly reduced signal intensity in NGF$^{R100W/wt}$ mice, compared with controls (Fig. 5*E*). To validate this measurement, we used the same anti-NGF primary antibody to titrate the different levels of NGF in the glabrous skin of NGF$^{+/+}$ and NGF$^{+/-}$ mice. Serial dilutions were used to demonstrate that the dose of antibody used for the experiment shown in Figure 5*E* can indeed detect the relative differences in NGF levels corresponding to the two genotypes, whereas, at a higher dilution, no significant difference was observed in NGF signal intensity (see Materials and Methods).

Taking into account the NGF reduction in the peripheral target sites of sensory fibers, we reasoned that exogenous administration of wild-type NGF could rescue the nociceptive deficit of NGF$^{R100W/wt}$ mice. To this aim, we performed a long-term NGF treatment, from embryonal life until 2 months of age, and analyzed the sensitivity of treated mice to capsaicin. A 21 d washout period after the last treatment was allowed (see Materials and Methods) to exclude an acute sensitizing action of NGF. This strategy proved successful in fully rescuing the nociceptive impairment of NGF$^{R100W/wt}$ mice (Fig. 5*F*).

This evidence indicates that the R100W mutation is responsible for multiple alterations in the pathway carrying nociceptive inputs, and that early treatment with wild-type NGF can restore pain perception.

### NGF$^{R100W}$ affects the secretion of wild-type NGF

The R100W mutation has been described to cause an impairment in the secretion of mature NGF in PC12 and COS cells (Larsson et al., 2009), but whether this is also true in human cells is not known. NGF is secreted as a homodimer. It is not known, however, whether NGF$^{R100W}$ affects the secretion of wild-type NGF when the two are coexpressed, as it happens in heterozygous NGF$^{R100W/wt}$ mice. We confirmed the secretion deficit of NGF$^{R100W}$ in human HEK cells (Fig. 6*A*). Strikingly, the secretion of wild-type, mature NGF was also impaired when coexpressed with NGF$^{R100W}$ (Fig. 6*A*). This suggested that a similar phenomenon might occur *in vivo* in NGF$^{R100W/wt}$ mice. Consistently, we found reduced total NGF levels of in plasma and brain from NGF$^{R100W/wt}$ mice (Fig. 6*B*,*C*).

### NGF$^{R100W/wt}$ mice show no learning and memory deficits

NGF is not only involved in the development and survival of sensory neurons, but is also a key regulator of brain development, in addition to being required for learning and memory processes, via its actions on CNS neuronal target cells such as forebrain cholinergic neurons (Chao, 2003).

We studied the learning and memory phenotype of NGF$^{R100W/wt}$ mice. Interestingly, NGF$^{R100W/wt}$ mice, tested in the Morris water maze (MWM), showed no difference in the learning performance, compared with wild-type controls (Fig. 7*A*), despite the lower brain NGF levels (Fig. 6*B*,*C*). A similar conclusion was drawn when challenging NGF$^{R100W/wt}$ mice and controls in the object recognition test. Indeed, NGF$^{R100W/wt}$ mice showed no significant differences in the exploratory activity and in the preference index (Fig. 7*C*,*D*), which indicate unaffected visuospatial recognition memory. Moreover, Schaffer collateral-CA1 long-term potentiation (LTP), a well established electrophysiological correlate of learning and memory (Davis et al., 1992), did not significantly differ in NGF$^{R100W/wt}$ mice from NGF$^{wt/wt}$ animals, thus supporting an intact hippocampal function (Fig. 7*E*,*F*).

Heterozygous NGF knock-out mice (mNGF$^{+/}$) are also characterized by lower brain levels of wild-type NGF (Chen et al., 1997), similar to NGF$^{R100W/wt}$ mice. In this case, as expected, mNGF$^{+/-}$ mice showed delayed learning in the MWM when compared with their controls (Fig. 7*B*). No significant differences in the latency to locate the platform where detected among the four experimental groups on day 1 (NGF$^{wt/wt}$, 100.560 ± 11.742 s; NGF$^{R100W/wt}$, 98.438 ± 9.919 s; NGF$^{+/+}$, 117.714 ± 2.286 s;

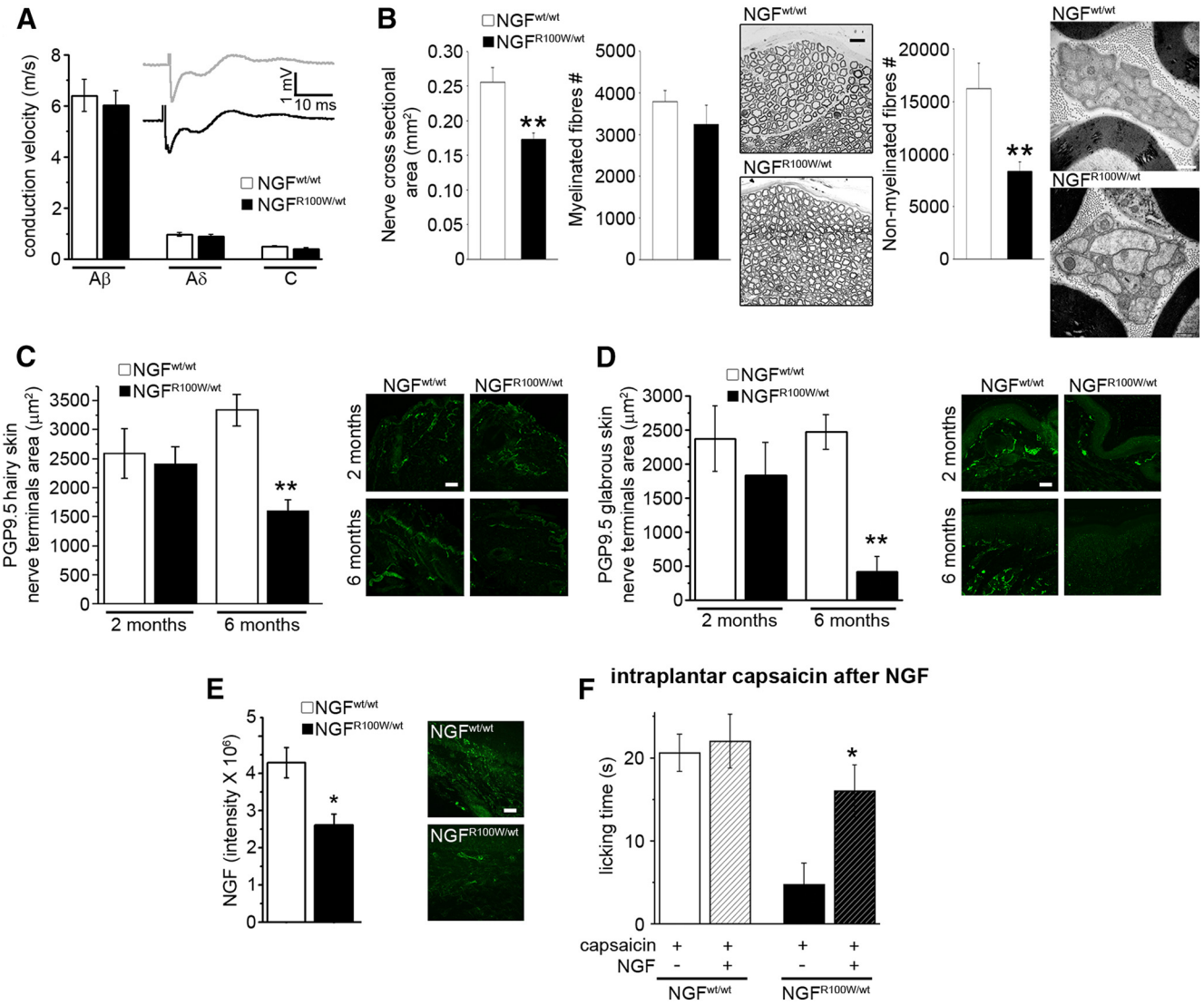


**Figure 5.** Reduced C-fiber density and skin innervation in NGF$^{R100W/wt}$ mice and rescue of nociceptive deficits by NGF$^{wt}$ treatment. ***A***, No alteration in conduction velocity of Aβ, Aδ, and C fibers in adult mice. Aβ fiber peak, Student's two-tailed *t* test ($t = 0.435$, $p = 0.669$); Aδ fiber peak, Student's two-tailed *t* test ($t = 0.737$, $p = 0.470$); C fiber peak, Student's two-tailed *t* test ($t = 1.629$, $p = 0.120$); NGF$^{wt/wt}$, $n = 10$; NGF$^{R100W/wt}$, $n = 11$ nerves. ***B***, Electron microscopy analysis of adult sciatic nerve reveals: significant reduction of cross-section area, Student's two-tailed *t* test ($t = 3.810$, $^{**}p = 0.004$); NGF$^{wt/wt}$, $n = 5$; NGF$^{R100W/wt}$, $n = 6$; unaffected number of myelinated axons, Student's two-tailed *t* test ($t = 0.983$, $p = 0.351$); NGF$^{wt/wt}$, $n = 5$; NGF$^{R100W/wt}$, $n = 6$, and significant reduction of slow nonmyelinated C axons, Student's two-tailed *t* test ($t = 3.295$, $^{**}p = 0.009$); NGF$^{wt/wt}$, $n = 5$; NGF$^{R100W/wt}$, $n = 6$. ***C***, Representative images and quantification of PGP9.5 expression show normal innervation at 2 months and a significant reduction at 6 months of age. Scale bar, 50 μm. 2 months, Student's two-tailed *t* test ($t = 0.340$, $p = 0.751$); NGF$^{wt/wt}$, $n = 3$; NGF$^{R100W/wt}$, $n = 3$; 6 months, Student's two-tailed *t* test ($t = 4.779$, $^{**}p = 0.004$); NGF$^{wt/wt}$, $n = 4$; NGF$^{R100W/wt}$, $n = 3$. ***D***, Age-dependent reduction in glabrous skin innervation. Scale bar, 50 μm. 2 months, Student's two-tailed *t* test ($t = 0.792$, $p = 0.473$); $n = 3$ for both groups. 6 months, Student's two-tailed *t* test ($t = 5.800$, $^{**}p = 0.002$); NGF$^{wt/wt}$, $n = 4$; NGF$^{R100W/wt}$, $n = 3$. ***E***, Decreased NGF levels in the glabrous skin of adult mice. Scale bar, 50 μm. Student's two-tailed *t* test ($t = 3.169$, $^{*}p = 0.034$); $n = 3$ for both groups. ***F***, Rescue of the sensitivity to capsaicin after treatment with mouse NGF$^{wt}$ from gestation until 2 months of age. NGF$^{wt/wt}$, Student's two-tailed *t* test ($t = 0.323$, $p = 0.754$); saline, $n = 5$; NGF, $n = 7$; NGF$^{R100W/wt}$, Student's two-tailed *t* test ($t = 2.764$, $^{*}p = 0.033$); saline, $n = 5$; NGF, $n = 4$.

NGF$^{+/-}$, 113.286 ± 3.887 s; ANOVA-1: $F_{(3,26)} = 1.565$, $p = 0.225$). This indicates a uniform initial performance in this task across different genotypes. In addition, mNGF$^{+/-}$ mice had impaired object recognition memory, despite unaffected exploratory behavior (Fig. 7*C*,*D*).

Cholinergic neurons are an NGF target population with an essential role in modulating learning and memory (Li et al., 1995). Thus, we analyzed the density of ChAT-immunoreactive neurons in the medial septum and striatum, and found them to be normal in NGF$^{R100W/wt}$ mice compared with controls (Fig. 7*G*,*H*). On the other hand, the density of ChAT-immunoreactive neurons in the same brain structures was decreased in mNGF$^{+/-}$ mice (Fig. 7*G*,*H*). These neuroanatomical data nicely correlate with the corresponding learning and memory behavioral phenotypes. Thus, the NGF$^{R100W}$ mutation, unlike *ngf* gene deletion, does not affect spatial learning and memory processes, in keeping with heterozygous R100W human carriers, who are reported to be cognitively normal (Einarsdottir et al., 2004).

## Discussion

Regulation of nociception and pain responses by NGF has long been a key area of research on this neurotrophin (Denk et al., 2017). This has spurred a significant translational interest for treating chronic pain conditions (Norman and McDermott, 2017). However, current understanding of these processes is still incomplete. Studying congenital insensitivity to pain disorders,

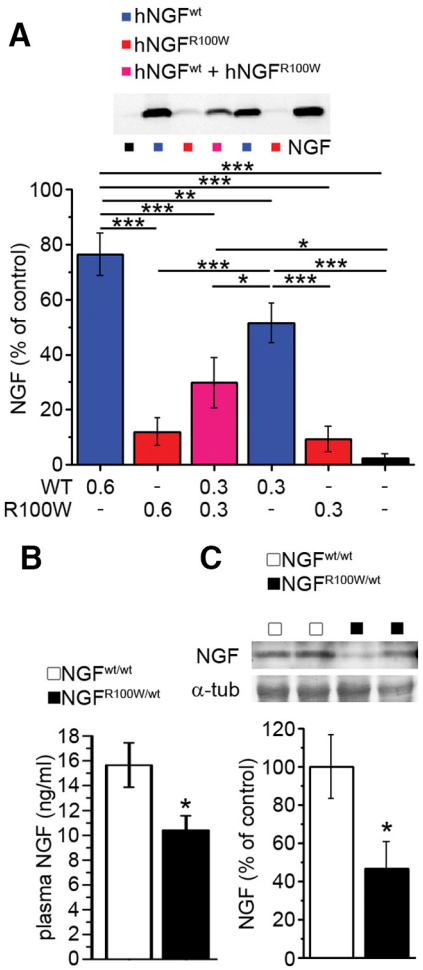


**Figure 6.** Impaired secretion and reduced NGF levels in the NGF$^{R100W}$ condition. ***A***, Impaired secretion of human NGF$^{R100W}$ in HEK293 cells transfected with the corresponding plasmid. Cotransfection of HEK293 cells with human NGF$^{wt}$ and human NGF$^{R100W}$ mimics the heterozygous condition, and shows a decrease in the secretion of human NGF$^{wt}$. ANOVA-1 ($F_{(5,24)} = 23.529$, $p < 0.001$) followed by Student–Newman–Keuls *post hoc* test, ***$p < 0.001$, **$p < 0.01$, *$p < 0.05$; NGF, $n = 5$; hNGF$^{wt}$ 0.6 $\mu$g, $n = 4$; hNGF$^{R100W}$ 0.6 $\mu$g, $n = 5$; hNGF$^{wt}$ + hNGF$^{R100W}$ 0.3 $\mu$g/each, $n = 3$; hNGF$^{wt}$ 0.3 $\mu$g, $n = 4$;hNGF$^{R100W}$ 0.3 $\mu$g, $n = 5$; mock, $n = 4$. ***B***, Reduced plasma NGF levels in NGF$^{R100W/wt}$ mice. Student's two-tailed *t* test (*$p = 0.031$); NGF$^{wt/wt}$, $n = 6$; NGF$^{R100W/wt}$, $n = 7$. ***C***, Lower abundance of NGF in brain extracts from NGF$^{R100W/wt}$ mice. Student's two-tailed *t* test ($t = 2.465$, *$p = 0.031$); NGF$^{wt/wt}$, $n = 6$; NGF$^{R100W/wt}$, $n = 7$.

such as HSAN V, offers a unique opportunity to fill this gap, through an alternative viewpoint on the NGF–TrkA axis involvement in chronic pain. In this regard, HSAN V has intriguing features, namely (1) the severe insensitivity to pain of homozygous patients, as opposed to the often clinically silent phenotype of heterozygous carriers; and (2) the absence of cognitive deficits, as opposed to HSAN IV patients, carrying TrkA mutations (Minde et al., 2004; Minde et al., 2009). We and others have previously elucidated that NGF$^{R100W}$ (1) is a TrkA biased agonist, failing to effectively engage p75$^{NTR}$ and activate the nociception-specific PLC-$\gamma$ pathway (Covaceuszach et al., 2010; Capsoni et al., 2011; Sung et al., 2018); (2) retains full neurotrophic activity via TrkA in a variety of cellular assays (Capsoni et al., 2011); and (3) disrupts processing of proNGF in cultures, leading to decreased secretion of mature NGF (Larsson et al., 2009; Fig. 6*A*). Moreover, topic injection of NGF$^{R100X}$ mutants does not induce acute pain (Capsoni et al., 2011; Sung et al., 2018; Fig. 4*D*). We have exploited these findings to obtain a "painless NGF" molecule for therapeutic purposes (Capsoni et al., 2017; Cattaneo and Capsoni, 2019), but how the features of NGF$^{R100W}$ contribute to the HSAN V phenotype is still far from clear. In particular, what are the consequences of this mutation on the overall architecture of pain-sensing structures and on nociceptive responses?

To shed light on these issues, we generated a new knock-in mouse line carrying the sequence encoding human NGF$^{R100W}$. In homozygosity, this mutation causes early postnatal lethality, rescued by NGF administration (Testa et al., 2019). This situation matches the effect of complete deletion of both *Ngf* alleles (Crowley et al., 1994) and its rescue by overexpression of *Ngf* (Harrison et al., 2004), thus pointing to reduced NGF bioavailability due to haploinsufficiency as the prevalent mechanistic explanation for the lethal phenotype of homozygous NGF$^{R100W/R100W}$ mice. Heterozygosity might mitigate the reduction in NGF bioavailability and reduce lethal developmental effects. Moreover, the vitality of NGF$^{R100W/wt}$ mice allows to look for further effects of NGF$^{R100W}$, including those possibly arising from peculiar signaling properties.

Heterozygous mice thrive normally and show no gross deficits, but display a reduction in nociception, accompanied by reduced skin innervation and altered density of nonmyelinated fibers, correlating with reduced NGF content in the skin.

The main DRG neuronal populations of NGF$^{R100W/wt}$ mice were unaffected and displayed a normal distribution in adults and newborns, which is in line with the full neurotrophic power of NGF$^{R100W}$. This rules out the possibility of an effect of the mutation on DRG development. However, the expression of key pain transduction-related molecules was altered. Triggered by this finding, we analyzed the global gene expression profile of DRGs by performing a transcriptomic study. NGF$^{R100W/wt}$ mice presented only subtle alterations, with a few hundred genes, belonging to gene categories involved in immune response, phagocytosis, and Rho-GTPase cycling, changed to a significant extent. Among the most affected genes were *TyroBP*/*DAP12* and *TLR2*, which modulate production of proinflammatory cytokines in neuropathic pain (Liu et al., 2012; Kobayashi et al., 2016). These interesting points deserve further investigation in the future, also considering the recent finding that microglia is a NGF target (Rizzi et al., 2018).

Another well established target of NGF, critically requiring TrkA signaling for proper development, is the sympathetic system (Levi-Montalcini and Booker, 1960; Glebova and Ginty, 2004; Kuruvilla et al., 2004). The SCG of NGF$^{R100W/wt}$ mice had a normal cell count, and peripheral sympathetic innervation of internal organs was similarly unaffected, further supporting the conclusion that NGF–TrkA signaling is intact in NGF$^{R100W/wt}$ mice.

The reactivity to algogens (capsaicin) and the sensitivity to non-noxious stimuli were decreased in NGF$^{R100W/wt}$ mice, correlating with the reduction in glabrous and hairy skin innervation, and in nonmyelinated fibers. These alterations fit with the lower NGF content in the target tissue (i.e., skin). Consistently, classical data show that NGF is not involved in establishing skin innervation during development, but is required for its maintenance in the adult (Davies et al., 1987), and the treatment of NGF$^{R100W/wt}$ mice with NGF$^{wt}$ was able to rescue their insensitivity to capsaicin-induced pain.

DRG neurons primed with NGF$^{R100W}$ are less prone to sensitization and show lower nociception-related biochemical responses than NGF$^{wt}$. In addition, NGF$^{R100W}$ was unable to induce mechanical allodynia *in vivo*. This is in line with the failure

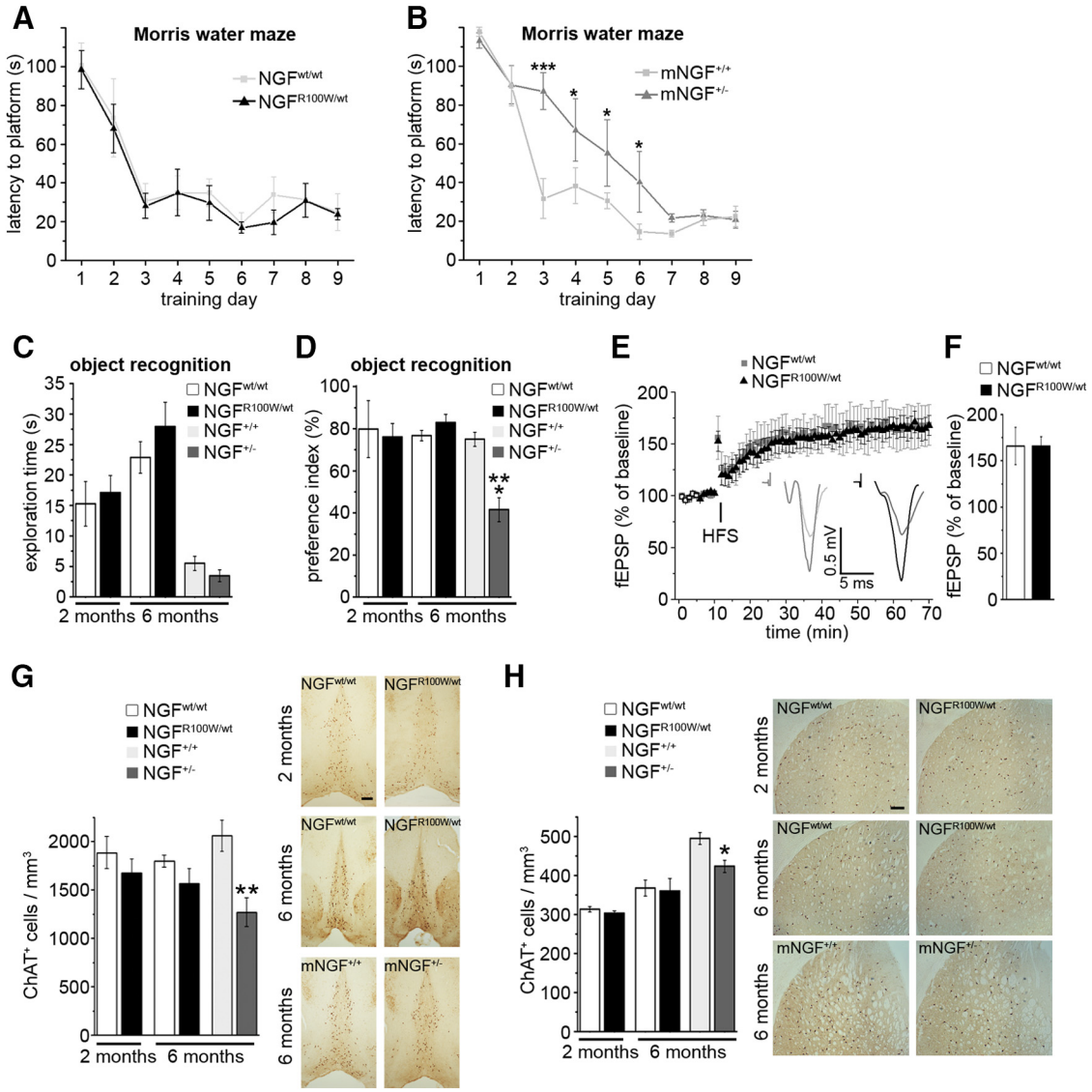


**Figure 7.** Normal cognitive function, hippocampal synaptic plasticity, and ChAT$^+$ neuron density in NGF$^{R100W/wt}$ mice. ***A***, Normal Morris water maze learning curve for adult NGF$^{R100W/wt}$ mice. ANOVA-2 with repeated measures (main effect of "training day": $F_{(8,112)} = 15.600$, $p < 0.001$). NGF$^{wt/wt}$, $n = 5$; NGF$^{R100W/wt}$, $n = 8$. ***B***, Delayed Morris water maze learning curve for mNGF$^{+/-}$ mice. ANOVA-2 with repeated measures ("training day" × "genotype" interaction, $F_{(8,123)} = 2.836$, $p = 0.007$), followed by Bonferroni *post hoc* test, *$p < 0.05$, ***$p < 0.001$; mNGF$^{+/+}$, $n = 7$; mNGF$^{+/-}$, $n = 7$. ***C***, Unimpaired Novel Object Recognition (NOR) sample phase for NGF$^{R100W/wt}$ and mNGF$^{+/-}$ mice. 2 months, Student's two-tailed *t* test: $t = 0.385$, $p = 0.704$; NGF$^{wt/wt}$, $n = 7$; NGF$^{R100W/wt}$, $n = 15$; 6 months, Student's *t* two-tailed test: $t = 1.094$, $p = 0.289$; NGF$^{wt/wt}$, $n = 10$; NGF$^{R100W/wt}$, $n = 9$; Student's two-tailed *t* test: $t = 1.303$, $p = 0.215$); mNGF$^{+/+}$, $n = 6$; mNGF$^{+/-}$, $n = 9$. ***D***, Unimpaired NOR test phase for NGF$^{R100W/wt}$ and visual recognition memory deficit for mNGF$^{+/-}$ mice. 2 months, Student's two-tailed *t* test: $t = 0.282$, $p = 0.780$; NGF$^{wt/wt}$, $n = 7$; NGF$^{R100W/wt}$, $n = 15$; 6 months, Student's *t* two-tailed test: $t = 1.453$, $p = 0.166$; NGF$^{wt/wt}$, $n = 10$; NGF$^{R100W/wt}$, $n = 8$; Student's two-tailed *t* test: $t = 4.450$, ***$p < 0.001$; mNGF$^{+/+}$, $n = 6$; mNGF$^{+/-}$, $n = 9$. ***E***, No significant differences in the time course of LTP at CA3–CA1 synapses induced by high-frequency stimulation (HFS) of the Schaffer collateral pathway between NGF$^{R100W/wt}$ and control mice. ANOVA-2 repeated measures (main effect of time, $F_{(69,966)} = 21.579$, $p < 0.001$; genotype, $F_{(1,966)} = 0.026$, $p = 0.875$; genotype × time interaction, $F_{(69,966)} = 0.156$, $p = 1.000$); $n = 9$ for each group. Representative traces show superimposed pre-HFS and post-HFS fEPSPs. ***F***, Comparable levels of LTP (obtained from averaging the last 10 min of recording) in NGF$^{R100W/wt}$ and NGF$^{wt/wt}$ mice. Student's two-tailed *t* test: $t = -0.001$, $p = 0.999$; $n = 9$ for each group. ***G***, ***H***, Normal septal ChAT$^+$ neuron density in basal forebrain and striatum in juvenile and adult NGF$^{R100W/wt}$ mice, and decreased density in mNGF$^{+/-}$ mice. Scale bar, 200 $\mu$m. Basal forebrain: 2 months: Student's two-tailed *t* test: $t = 0.958$, $p = 0.375$; NGF$^{wt/wt}$, $n = 4$; NGF$^{R100W/wt}$, $n = 4$; 6 months: Student's two-tailed *t* test: $t = 1.271$, $p = 0.278$; NGF$^{wt/wt}$, $n = 3$; NGF$^{R100W/wt}$, $n = 4$; Student's two-tailed *t* test: $t = 3.529$, **$p = 0.010$; mNGF$^{+/+}$, $n = 5$; mNGF$^{+/-}$, $n = 4$. Striatum: 2 months: Student's two-tailed *t* test: $t = 1.144$, $p = 0.296$; NGF$^{wt/wt}$, $n = 4$; NGF$^{R100W/wt}$, $n = 4$; 6 months: Student's two-tailed *t* test: $t = 0.180$, $p = 0.864$; NGF$^{wt/wt}$, $n = 3$; NGF$^{R100W/wt}$, $n = 4$; Student's two-tailed *t* test: $t = 3.212$, *$p = 0.015$; mNGF$^{+/+}$, $n = 5$; mNGF$^{+/-}$, $n = 4$.

of NGF$^{R100W}$ application to potentiate H$^+$-evoked responses in DRG cultures (Sung et al., 2018) and extends data showing that NGF$^{R100W}$ impacts nociceptive, but not trophic functions of NGF (Capsoni et al., 2011; Sung et al., 2018). Binding of NGF to p75$^{NTR}$ is required for the upregulation of bradykinin receptor expression (Petersen et al., 1998) and NGF$^{R100W}$ has a reduced affinity to this receptor (Covaceuszach et al., 2010; Sung et al., 2018). Interestingly, reduced p75$^{NTR}$ binding can explain the common features of NGF$^{R100W/wt}$ mice with p75$^{NTR-/-}$ mice, which have reduced nociception and skin innervation, despite normal DRG structure (Bergmann et al., 1997). This strongly suggests that the molecular mechanism for the reduced activation of pain sensitization pathways by NGF$^{R100W}$ is a differential engagement of TrkA and p75$^{NTR}$ receptors.

Congenital insensitivity to pain is usually explained by defective nociceptor development or function (Chen et al., 2015; Mi-

nett et al., 2015; Nahorski et al., 2015), whereas nociceptors develop normally in HSAN V mice. Therefore, the reduced sensitizing activity of NGF$^{R100W}$ may contribute to explain the HSAN V phenotype.

Reduced NGF levels can explain the lethality of homozygous NGF$^{R100W/R100W}$ mice (Testa et al., 2019), thus mimicking the lethality of mNGF$^{-/-}$ mice (Crowley et al., 1994). Under heterozygosity, the mutation has a milder impact, both in human carriers (Perini et al., 2016) and mice (our data), despite reduced plasma and brain NGF (Fig. 6*B*,*C*).

HSAN IV, differently from HSAN V, is characterized by mental retardation and anhidrosis (Indo, 2001; Capsoni, 2014), showing that mutations in the ligand and in its receptor are not completely overlapping. Indeed, heterozygous mice (our data) and humans (Minde et al., 2009) show normal cognitive performance and normal density of cholinergic neurons, in striking contrast to mNGF$^{+/-}$ mice, further demonstrating that NGF$^{R100W}$ retains a full neurotrophic potential in the CNS and suggesting a specific effect of the R100W mutation on nociceptive pathways. In this regard, it is worth noticing that conditional deletion of *Ngf* or *TrkA* in nestin$^{+}$ neurons causes a reduction of ChAT$^{+}$ neurons in the medial septum, but not in the striatum (Müller et al., 2012). Likewise, deletion of *TrkA* from *dlx5/6*-expressing neurons caused a reduction in ChAT expression in the basal forebrain, but not in the striatum, along with mild cognitive deficits (Sanchez-Ortiz et al., 2012). We observed no cholinergic deficit in NGF$^{R100W/wt}$ mice, whereas this was detected in NGF$^{+/-}$ mice not only in the medial septum, but also in the striatum. These differences could be explained either by (1) the unaltered neurotrophic activity of NGF$^{R100W}$ or by (2) the reduction in glial NGF/TrkA production/signaling caused by the global heterozygous deletion in NGF$^{+/-}$ mice, which in conditional knock-out mice occurred only in the neuronal lineage. This suggests a contribution of microglia to NGF actions in the CNS, which is in agreement with the recent finding that microglia is an NGF target cell in the brain (Rizzi et al., 2018). On the other hand, nociception and the associated pathways were not analyzed in detail in neuron-specific *Ngf* and *TrkA* conditional knock-out mice (Müller et al., 2012; Sanchez-Ortiz et al., 2012).

Since NGF is a homodimer, it is not known whether heterodimers between NGF$^{wt}$ and NGF$^{R100W}$ protomers can be formed, and what are their peripheral and central functional properties. This possibility is suggested by the decreased secretion of NGF$^{wt}$, when coexpressed with NGF$^{R100W}$, and, therefore, it is tempting to speculate that the NGF$^{R100W}$ chain exerts a dominant-negative effect on wild-type chains. Considering that the expression of NGF$^{R100W}$ alone also results in reduced secretion, it is conceivable that the presence of this particular mutant, leading to either the formation of NGF$^{wt}$-NGF$^{R100W}$ heterodimers or to a mixture of NGF$^{wt}$-NGF$^{wt}$ and NGF$^{R100W}$-NGF$^{R100W}$ homodimers can affect the secretion/processing quality control systems, thus resulting in reduced extracellular release. An antibody against the mutant NGF chain would be required to demonstrate the presence of heterodimers, which will be the focus of future research efforts.

By generating a new mouse model for the human NGF$^{R100W}$ mutation in the heterozygous state, we have provided new insights into the HSAN V "painlessness" condition, which call for future study of its potential as a new tool to dissect the multifaceted roles of NGF in the nervous system. In addition, the "painless" properties of NGF$^{R100W}$ hold promising potential to design much needed strategies to treat chronic pain states.

## References


Apfel SC (2002) Nerve growth factor for the treatment of diabetic neuropathy: what went wrong, what went right, and what does the future hold? Int Rev Neurobiol 50:393–413.

Apfel SC, Arezzo JC, Brownlee M, Federoff H, Kessler JA (1994) Nerve growth factor administration protects against experimental diabetic sensory neuropathy. Brain Res 634:7–12.

Axelsson HE, Minde JK, Sonesson A, Toolanen G, Högestätt ED, Zygmunt PM (2009) Transient receptor potential vanilloid 1, vanilloid 2 and melastatin 8 immunoreactive nerve fibers in human skin from individuals with and without norrbottnian congenital insensitivity to pain. Neuroscience 162:1322–1332.

Barone I, Melani R, Mainardi M, Scabia G, Scali M, Dattilo A, Ceccarini G, Vitti P, Santini F, Maffei L, Pizzorusso T, Maffei M (2018) Fluoxetine modulates the activity of hypothalamic POMC neurons via mTOR signaling. Mol Neurobiol 55:9267–9279.

Bergmann I, Priestley JV, McMahon SB, Bröcker EB, Toyka KV, Koltzenburg M (1997) Analysis of cutaneous sensory neurons in transgenic mice lacking the low affinity neurotrophin receptor p75. Eur J Neurosci 9:18–28.

Bonnington JK, McNaughton PA (2003) Signalling pathways involved in the sensitisation of mouse nociceptive neurones by nerve growth factor. J Physiol 551:433–446.

Capsoni S (2014) From genes to pain: nerve growth factor and hereditary sensory and autonomic neuropathy type V. Eur J Neurosci 39:392–400.

Capsoni S, Covaceuszach S, Marinelli S, Ceci M, Bernardo A, Minghetti L, Ugolini G, Pavone F, Cattaneo A (2011) Taking pain out of NGF: a "painless" NGF mutant, linked to hereditary sensory autonomic neuropathy type V, with full neurotrophic activity. PLoS One 6:e17321.

Capsoni S, Malerba F, Carucci NM, Rizzi C, Criscuolo C, Origlia N, Calvello M, Viegi A, Meli G, Cattaneo A (2017) The chemokine CXCL12 mediates the anti-amyloidogenic action of painless human nerve growth factor. Brain 140:201–217.

Cattaneo A, Capsoni S (2019) Painless nerve growth factor: a TrkA biased agonist mediating a broad neuroprotection via its actions on microglia cells. Pharmacol Res 139:17–25.

Chao MV (2003) Neurotrophins and their receptors: a convergence point for many signalling pathways. Nat Rev Neurosci 4:299–309.

Chen KS, Nishimura MC, Armanini MP, Crowley C, Spencer SD, Phillips HS (1997) Disruption of a single allele of the nerve growth factor gene results in atrophy of basal forebrain cholinergic neurons and memory deficits. J Neurosci 17:7288–7296.

Chen YC, Auer-Grumbach M, Matsukawa S, Zitzelsberger M, Themistocleous AC, Strom TM, Samara C, Moore AW, Cho LT, Young GT, Weiss C, Schabhüttl M, Stucka R, Schmid AB, Parman Y, Graul-Neumann L, Heinritz W, Passarge E, Watson RM, Hertz JM, et al (2015) Transcriptional regulator PRDM12 is essential for human pain perception. Nat Genet 47:803–808.

Chuang HH, Prescott ED, Kong H, Shields S, Jordt SE, Basbaum AI, Chao MV, Julius D (2001) Bradykinin and nerve growth factor release the capsaicin receptor from PtdIns(4,5)P2-mediated inhibition. Nature 411:957–962.

Covaceuszach S, Capsoni S, Marinelli S, Pavone F, Ceci M, Ugolini G, Vignone D, Amato G, Paoletti F, Lamba D, Cattaneo A (2010) In vitro receptor binding properties of a "painless" NGF mutein, linked to hereditary sensory autonomic neuropathy type V. Biochem Biophys Res Commun 391:824–829.

Crerar H, Scott-Solomon E, Bodkin-Clarke C, Andreassi C, Hazbon M, Logie E, Cano-Jaimez M, Gaspari M, Kuruvilla R, Riccio A (2019) Regulation of NGF signaling by an axonal untranslated mRNA. Neuron 102:553–563.e8.

Crowley C, Spencer SD, Nishimura MC, Chen KS, Pitts-Meek S, Armanini MP, Ling LH, McMahon SB, Shelton DL, Levinson AD (1994) Mice lacking nerve growth factor display perinatal loss of sensory and sympathetic neurons yet develop basal forebrain cholinergic neurons. Cell 76:1001–1011.

Davies AM, Bandtlow C, Heumann R, Korsching S, Rohrer H, Thoenen H (1987) Timing and site of nerve growth factor synthesis in developing skin in relation to innervation and expression of the receptor. Nature 326:353–358.

Davis S, Butcher SP, Morris RG (1992) The NMDA receptor antagonist D-2-amino-5-phosphonopentanoate (D-AP5) impairs spatial learning

and LTP in vivo at intracerebral concentrations comparable to those that block LTP *in vitro*. J Neurosci 12:21–34.
Denk F, Bennett DL, McMahon SB (2017) Nerve growth factor and pain mechanisms. Annu Rev Neurosci 40:307–325.
Einarsdottir E, Carlsson A, Minde J, Toolanen G, Svensson O, Solders G, Holmgren G, Holmberg D, Holmberg M (2004) A mutation in the nerve growth factor beta gene (NGFB) causes loss of pain perception. Hum Mol Genet 13:799–805.
Glebova NO, Ginty DD (2004) Heterogeneous requirement of NGF for sympathetic target innervation *in vivo*. J Neurosci 24:743–751.
Harrison SM, Davis BM, Nishimura M, Albers KM, Jones ME, Phillips HS (2004) Rescue of NGF-deficient mice I: transgenic expression of NGF in skin rescues mice lacking endogenous NGF. Brain Res Mol Brain Res 122:116–125.
Indo Y (2001) Molecular basis of congenital insensitivity to pain with anhidrosis (CIPA): mutations and polymorphisms in TRKA (NTRK1) gene encoding the receptor tyrosine kinase for nerve growth factor. Hum Mutat 18:462–471.
Kobayashi M, Konishi H, Sayo A, Takai T, Kiyama H (2016) TREM2/DAP12 signal elicits proinflammatory response in microglia and exacerbates neuropathic pain. J Neurosci 36:11138–11150.
Kuruvilla R, Zweifel LS, Glebova NO, Lonze BE, Valdez G, Ye H, Ginty DD (2004) A neurotrophin signaling cascade coordinates sympathetic neuron development through differential control of TrkA trafficking and retrograde signaling. Cell 118:243–255.
Lane NE, Schnitzer TJ, Birbara CA, Mokhtarani M, Shelton DL, Smith MD, Brown MT (2010) Tanezumab for the treatment of pain from osteoarthritis of the knee. N Engl J Med 363:1521–1531.
Larsson E, Kuma R, Norberg A, Minde J, Holmberg M (2009) Nerve growth factor R221W responsible for insensitivity to pain is defectively processed and accumulates as proNGF. Neurobiol Dis 33:221–228.
Levi-Montalcini R (1987) The nerve growth factor 35 years later. Science 237:1154–1162.
Levi-Montalcini R, Booker B (1960) Destruction of the sympathetic ganglia in mammals by an antiserum to a nerve-growth protein. Proc Natl Acad Sci U S A 46:384–391.
Levi-Montalcini R, Skaper SD, Dal Toso R, Petrelli L, Leon A (1996) Nerve growth factor: from neurotrophin to neurokine. Trends Neurosci 19:514–520.
Lewin GR, Ritter AM, Mendell LM (1993) Nerve growth factor-induced hyperalgesia in the neonatal and adult rat. J Neurosci 13:2136–2148.
Lewin GR, Lechner SG, Smith ES (2014) Nerve growth factor and nociception: from experimental embryology to new analgesic therapy. Handb Exp Pharmacol 220:251–282.
Li Y, Holtzman DM, Kromer LF, Kaplan DR, Chua-Couzens J, Clary DO, Knüsel B, Mobley WC (1995) Regulation of TrkA and ChAT expression in developing rat basal forebrain: evidence that both exogenous and endogenous NGF regulate differentiation of cholinergic neurons. J Neurosci 15:2888–2905.
Liu T, Gao YJ, Ji RR (2012) Emerging role of toll-like receptors in the control of pain and itch. Neurosci Bull 28:131–144.
McMahon SB, Bennett DL, Priestley JV, Shelton DL (1995) The biological effects of endogenous nerve growth factor on adult sensory neurons revealed by a trkA-IgG fusion molecule. Nat Med 1:774–780.
Minde J, Toolanen G, Andersson T, Nennesmo I, Remahl IN, Svensson O, Solders G (2004) Familial insensitivity to pain (HSAN V) and a mutation in the NGFB gene. A neurophysiological and pathological study. Muscle Nerve 30:752–760.
Minde J, Andersson T, Fulford M, Aguirre M, Nennesmo I, Remahl IN, Svensson O, Holmberg M, Toolanen G, Solders G (2009) A novel NGFB point mutation: a phenotype study of heterozygous patients. J Neurol Neurosurg Psychiatry 80:188–195.
Minett MS, Pereira V, Sikandar S, Matsuyama A, Lolignier S, Kanellopoulos AH, Mancini F, Iannetti GD, Bogdanov YD, Santana-Varela S, Millet Q, Baskozos G, MacAllister R, Cox JJ, Zhao J, Wood JN (2015) Endogenous opioids contribute to insensitivity to pain in humans and mice lacking sodium channel Nav1.7. Nat Commun 6:8967.
Minnone G, De Benedetti F, Bracci-Laudiero L (2017) NGF and its receptors in the regulation of inflammatory response. Int J Mol Sci 18:E1028.
Mitra S, Behbahani H, Eriksdotter M (2019) Innovative Therapy for Alzheimer's Disease-With Focus on Biodelivery of NGF. Front Neurosci 13:38.
Molliver DC, Wright DE, Leitner ML, Parsadanian AS, Doster K, Wen D, Yan Q, Snider WD (1997) IB4-binding DRG neurons switch from NGF to GDNF dependence in early postnatal life. Neuron 19:849–861.
Müller M, Triaca V, Besusso D, Costanzi M, Horn JM, Koudelka J, Geibel M, Cestari V, Minichiello L (2012) Loss of NGF-TrkA signaling from the CNS is not sufficient to induce cognitive impairments in young adult or intermediate-aged mice. J Neurosci 32:14885–14898.
Nahorski MS, Chen YC, Woods CG (2015) New mendelian disorders of painlessness. Trends Neurosci 38:712–724.
Norman BH, McDermott JS (2017) Targeting the nerve growth factor (NGF) pathway in drug discovery: potential applications to new therapies for chronic pain. J Med Chem 60:66–88.
Paoletti F, Malerba F, Ercole BB, Lamba D, Cattaneo A (2015) A comparative analysis of the structural, functional and biological differences between mouse and human nerve growth factor. Biochim Biophys Acta 1854:187–197.
Perini I, Tavakoli M, Marshall A, Minde J, Morrison I (2016) Rare human nerve growth factor-beta mutation reveals relationship between C-afferent density and acute pain evaluation. J Neurophysiol 116:425–430.
Petersen M, Segond von Banchet G, Heppelmann B, Koltzenburg M (1998) Nerve growth factor regulates the expression of bradykinin binding sites on adult sensory neurons via the neurotrophin receptor p75. Neuroscience 83:161–168.
Pittenger G, Vinik A (2003) Nerve growth factor and diabetic neuropathy. Exp Diabesity Res 4:271–285.
Purves D, Snider WD, Voyvodic JT (1988) Trophic regulation of nerve cell morphology and innervation in the autonomic nervous system. Nature 336:123–128.
Ritchie ME, Phipson B, Wu D, Hu Y, Law CW, Shi W, Smyth GK (2015) limma powers differential expression analyses for RNA-sequencing and microarray studies. Nucleic Acids Res 43:e47.
Rizzi C, Tiberi A, Giustizieri M, Marrone MC, Gobbo F, Carucci NM, Meli G, Arisi I, D'Onofrio M, Marinelli S, Capsoni S, Cattaneo A (2018) NGF steers microglia toward a neuroprotective phenotype. Glia 66:1395–1416.
Sanchez-Ortiz E, Yui D, Song D, Li Y, Rubenstein JL, Reichardt LF, Parada LF (2012) TrkA gene ablation in basal forebrain results in dysfunction of the cholinergic circuitry. J Neurosci 32:4065–4079.
Shboul M, Roschger P, Ganger R, Paschalis L, Rokidi S, Zandieh S, Behunova J, Muschitz C, Fahrleitner-Pammer A, Ng AYJ, Tohari S, Venkatesh B, Bonnard C, Reversade B, Klaushofer K, Al Kaissi A (2019) Bone matrix hypermineralization associated with low bone turnover in a case of Nasu-Hakola disease. Bone 123:48–55.
Skaper SD (2017) Nerve growth factor: a neuroimmune crosstalk mediator for all seasons. Immunology 151:1–15.
Sung K, Ferrari LF, Yang W, Chung C, Zhao X, Gu Y, Lin S, Zhang K, Cui B, Pearn ML, Maloney MT, Mobley WC, Levine JD, Wu C (2018) Swedish nerve growth factor mutation (NGF(R100W)) defines a role for TrkA and p75(NTR) in nociception. J Neurosci 38:3394–3413.
Svensson P, Cairns BE, Wang K, Arendt-Nielsen L (2003) Injection of nerve growth factor into human masseter muscle evokes long-lasting mechanical allodynia and hyperalgesia. Pain 104:241–247.
Szklarczyk D, Franceschini A, Wyder S, Forslund K, Heller D, Huerta-Cepas J, Simonovic M, Roth A, Santos A, Tsafou KP, Kuhn M, Bork P, Jensen LJ, von Mering C (2015) STRING v10: protein-protein interaction networks, integrated over the tree of life. Nucleic Acids Res 43:D447–D452.
Taneda K, Tominaga M, Tengara S, Ogawa H, Takamori K (2010) Neurotropin inhibits both capsaicin-induced substance P release and nerve growth factor-induced neurite outgrowth in cultured rat dorsal root ganglion neurones. Clin Exp Dermatol 35:73–77.
Testa G, Calvello M, Cattaneo A, Capsoni S (2019) Cholinergic striatal neurons are increased in HSAN V homozygous mice despite reduced NGF bioavailability. Biochem Biophys Res Commun 509:763–766.
Ugolini G, Marinelli S, Covaceuszach S, Cattaneo A, Pavone F (2007) The function neutralizing anti-TrkA antibody MNAC13 reduces inflammatory and neuropathic pain. Proc Natl Acad Sci U S A 104:2985–2990.
Wetzel C, Hu J, Riethmacher D, Benckendorff A, Harder L, Eilers A, Moshourab R, Kozlenkov A, Labuz D, Caspani O, Erdmann B, Machelska H, Heppenstall PA, Lewin GR (2007) A stomatin-domain protein essential for touch sensation in the mouse. Nature 445:206–209.
Zhang X, Huang J, McNaughton PA (2005) NGF rapidly increases membrane expression of TRPV1 heat-gated ion channels. EMBO J 24:4211–4223.
Zimmerman A, Bai L, Ginty DD (2014) The gentle touch receptors of mammalian skin. Science 346:950–954.